

Chapter 2

Photo-Luminescent Materials: Down-Conversion, Quantum Cutting, Up-Conversion, Photo-Avalanche, Core@ Shell Nanostructures



Ruchi Agrawal, Manas Srivastava, and Raghmani S. Ningthoujam

2.1 Introduction

Photo-luminescent materials are materials, which can emit light after absorption of suitable light (Ningthoujam et al. 2012, 2022; Yadav and Ningthoujam 2021; Curie 1963; Blasse and Grabmaier 1994; Brabec et al. 2003; Simmons et al. 2000). Upon excitation, electrons in the ground state get excited to a higher energy state. Once excitation source is removed, the electrons in the higher energy state return to the ground state giving rise to emission. Materials can be of solid, liquid and gas. Solid materials can be amorphous, glass, plastic, single-crystalline, nanocrystalline and polycrystalline. Examples of solid materials are ZnO, SnO₂, TiO₂, YVO₄, CaMoO₄, PbSe, InP, PbS, GaN, InGaN, etc. (Singh et al. 2009a; Sahu et al. 2012a; Ghosh et al. 2011; Ningthoujam et al. 2007a, 2009a, 2017; Ganapathi et al. 2022; Luwang et al. 2010; Ningthoujam and Kulshreshtha 2009; Haider et al. 2019; Longo et al. 2011; Chen et al. 2020; Mamiyev and Balayeva 2023; Strite and Morkoç 1992; Sheen et al. 2022). Liquid samples are dyes dissolved in water or alcohol. Examples are Fluorescein isothiocyanate (FITC) dissolved in water (Chaganti et al. 2018; Joshi et al. 2022a), Fluorinated Boron-Dipyrromethene (BODIPY), 4',6-diamidino-2-phenylindole (DAPI) and Curcumin dissolved in water/alcohol (Boens et al. 2012; Omelon et al. 2016; Shetty et al. 2015). In order to change/tune the luminescence intensity or peaks, sometimes, 2 or 3 systems of different phosphor materials or ions are interfaced to form composite or core@shell or substitution (Pan et al. 2018; Shao et al. 2017; Parchur et al. 2012a; Dutta et al. 2012). Also, many ions

R. Agrawal · M. Srivastava · R. S. Ningthoujam (✉)
Chemistry Division, Bhabha Atomic Research Centre, Mumbai 400085, India
e-mail: rsn@barc.gov.in

R. Agrawal · R. S. Ningthoujam
Homi Bhabha National Institute, Anushakti nagar, Mumbai 400094, India

are doped to the host to change luminescence or control luminescence behaviour. One example is Tl-doped NaCl used in dosimetry (Takizawa et al. 2021). The ‘d’ or ‘f’ block ions are doped to host. Examples of ‘d’ block ion doped material is host: Mn or host: Cr (Ahmed 2017; Loksha et al. 2023). The ‘f’ block ions doped materials include the followings: $\text{ZnO}_2:\text{Ln}^{3+}$, $\text{SnO}_2:\text{Ln}^{3+}$, $\text{ZrO}_2:\text{Eu}^{3+}$, $\text{TiO}_2:\text{Ln}^{3+}$, $\text{CaMoO}_4:\text{Ln}^{3+}$, $\text{AVO}_4:\text{Ln}^{3+}$ ($A = \text{Y, La, Gd, Lu}$), and $\text{APO}_4:\text{Ln}^{3+}$, etc. (Ningthoujam et al. 2007b, c, 2008a, b, 2009a, b, c; Gajbhiye et al. 2008; Singh et al. 2008a, b, 2009b, c, 2010, 2012, 2014a, b, 2015; Rao et al. 2008; Srinivasu et al. 2009; Yaiphaba et al. 2010a, b, c; Phaomei et al. 2010, 2011a, b, 2013; Shukla et al. 2010; Lahiri et al. 2010; Singh and Ningthoujam 2010, 2011; Ningthoujam 2010, 2013; Meetei et al. 2012; Sahu et al. 2012b, 2014; Parchur et al. 2012b, 2014; Parchur and Ningthoujam 2012a; Loitongbam et al. 2013; Prasad et al. 2013; Okram et al. 2014). Here, $\text{Ln}^{3+} = \text{Ce}^{3+}, \text{Eu}^{3+}, \text{Gd}^{3+}, \text{Pr}^{3+}, \text{Sm}^{3+}, \text{Ho}^{3+}, \text{Dy}^{3+}, \text{Tb}^{3+}, \text{Er}^{3+}, \text{Yb}^{3+}$. In some cases, 2 or more dopants of different elements are also co-doped to host. There are many phosphors in the form of liquid crystals (Wang et al. 2015). Also, shape and size engineering can bring many photo-luminescent materials for advanced flexible materials in the forms of thin films, single crystals, poly-crystals, amorphous, etc. Perovskite compounds (ABO_3) of pure inorganic, organic, inorganic–organic or lanthanide doped particles (quantum dots, polycrystalline) have been extensively studied for their either excellent luminescence emission, high quantum yields or ferroelectrics (Tai et al. 2019; Ye et al. 2018; Wang et al. 2020). A few examples are MDABCO (N-methyl-N'-diazabicyclo[2.2.2]octonium)–ammonium, $\text{HC}(\text{NH}_2)_2\text{PbBr}_3$, CsPbX_3 ($X = \text{Cl, Br, I}$). Organic phosphors are very light as compared to inorganic phosphors.

There are two terms: sensitizer and activator in luminescence (Ningthoujam et al. 2012; Yadav and Ningthoujam 2021). The sensitizer is ion/species, which has high absorption cross-section and its emission is absorbed by another species or ion known as activator through an energy transfer process (radiative or non-radiative process). In this way, activator can produce an improved emission intensity. One example is $\text{APO}_4:\text{Ce-Tb}$ ($A = \text{La, Y, Gd}$) (Ningthoujam et al. 2012; Yadav and Ningthoujam 2021; Phaomei et al. 2011a; Sahu et al. 2014). Ce^{3+} ions have high absorption cross-section in UV region (250–280 nm) due to allowed transition (f-d transition) and emit a broad emission in 320–360 nm. On the other hand, Tb^{3+} ions have low absorption cross-section in 320–400 nm due to Laporte forbidden (f-f transition). By absorption of UV light at 250 nm by Ce^{3+} , its luminescence intensity at 350 nm is absorbed by Tb^{3+} ions and thus an enhanced luminescence intensity from Tb^{3+} can be obtained. In general, Förster and Dexter energy transfer processes can occur in sensitizer to activator combination (Cravenco et al. 2020; Lakowicz 2006). Luminescence intensity of activator decreases due to the presence of quencher. This can be brought by the addition of a large number of activators or presence of magnetic ions (Ningthoujam et al. 2012). Increase of activator ions in rare-earth ions doped systems reduces luminescence intensity. This is known as concentration quenching effect.

In the study of luminescence decay, various lifetimes (τ) are observed from the different materials: ns (nanoseconds), μs (microseconds), ms (milliseconds), minutes and hours (Ningthoujam et al. 2012; Curie 1963; Blasse and Grabmaier 1994; Lakowicz 2006). Most semiconductors, insulators or organic phosphors exhibit

lifetimes in ns range. The rare-earth doped semiconductors or insulators exhibit lifetimes in μs –ms range. Some insulators doped with Ln^{3+} , Mn^{2+} or Cr^{3+} can exhibit lifetimes in minutes to hours after removal of the excitation source. This is considered as persistence or delay luminescence (Zhuang et al. 2014; Sharma et al. 2023).

In some cases, the excitation energy is less than that of emitted light and the process is known as frequency up-conversion. Here, suitable light in NIR (near infrared) region is used to excite materials and these excited electrons are again brought to the higher excited state through many processes (energy transfer). Examples are $\text{NaYF}_4:\text{Er}$, Yb , $\text{NaGdF}_4:\text{Er}$, Yb , and $\text{LaF}_3:\text{Ho-Yb}$, etc. (Auzel 2004). Under 980 nm excitation, visible emission is observed. Similarly, organic compounds ($[\text{Ru}(\text{dmb})_3]^{2+}/\text{DPA}$ system; $\text{dmb} = \text{tris}(4,4'\text{-dimethyl-2,2'}\text{-bipyridine})$; $\text{DPA} = 9,10\text{-diphenyl-anthracene}$) can show the blue light under green light excitation (i.e., up-conversion) (Singh-Rachford and Castellano 2010).

There are many examples of photo-luminescent materials in the form of organic molecules, polymers, inorganic molecules, host–guest molecules, supermolecules, metal–organic frameworks, antenna-types molecules, hybrid, composite and core@shell nanoparticles. These luminescent materials are used in many applications such as LEDs (light emitting diodes), power saving, security ink, imaging, cancer detection, biological imaging and therapy, etc. (Ningthoujam et al. 2012, 2022; Yadav and Ningthoujam 2021; Curie 1963; Blasse and Grabmaier 1994; Kumari et al. 2019a, b, 2021, 2023). Such materials can be grouped into 2: down-conversion and up-conversion luminescent materials.

In this chapter, frequency down-conversion and up-conversion luminescent materials will be discussed with many examples. The quantum cutting process is addressed here. In the last section, proximity effects due to core@shell nanostructures are provided. The effects of particle size on luminescence intensity are mentioned by taking a few examples.

2.2 Types of Photoluminescence Process

On the basis of the frequency conversion from excitation to emission, there are 2 types of photoluminescence process: Frequency down-conversion and Frequency up-conversion (Ningthoujam et al. 2012, 2022; Yadav and Ningthoujam 2021; Curie 1963; Blasse and Grabmaier 1994).

2.2.1 Frequency Down-Conversion

Frequency down-conversion optical materials are materials, which are able to convert an absorbed light into an emitted light of lower energy. Here, the excitation energy is more than the emitted energy or wavelength of the excitation energy is less than that

Types of Photoluminescence

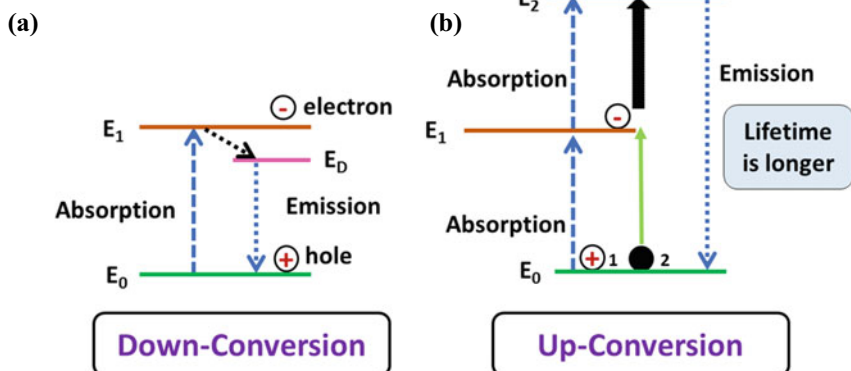


Fig. 2.1 Two types of photoluminescence process: **a** Frequency down-conversion and **b** Frequency up-conversion

of emitted light ($\lambda_{em} > \lambda_{ex}$). The schematic diagram illustrating frequency down-conversion is shown in Fig. 2.1a. At initial stage, ground state electrons absorb light and electrons go from the ground state to the excited state ($E_0 \rightarrow E_1$), hole is formed at the ground state and excited electrons at E_1 can come back to the ground state radiatively or non-radiatively. If there are defects or impurities, excited electrons stay sometime at the level (E_D), which is just below E_1 . Then emission occurs. Here, the emitted energy is less than the absorbed energy. Here, 2 types of frequency down-conversion luminescent materials can be seen.

2.2.1.1 Normal (or Down-Shifting)

This was observed in organic compounds, semiconductors, d- and f- block ions and metal–ligand charge transfer systems. A few examples of organic compounds are anthracene, 4',6-diamidino-2-phenylindole (DAPI), Fluorescein isothiocyanate (FITC), fluorinated boron-dipyrromethene (BODIPY), dyes, curcumin, etc. Metal centre-organic molecule complexes are iron propylene and haemoglobin. Host–guest complexes include supermolecular molecules, in which dye molecules are trapped inside host molecule. Examples of d block containing inorganic compounds are the first-row transition metal complexes, zirconium and hafnium complexes with pyridine dipyrroliide ligands (Wegeberg and Wenger 2021; Leary et al. 2023). Examples of f block containing inorganic compounds are lanthanide complexes and lanthanide–titanium oxo clusters (Hasegawa et al. 2022; Tanner and Pan 2009; Chen et al. 2019; Li and Li 2021). In organic compounds, π - bonds conjugation helps in the reduction of energy gap between HOMO (highest occupied molecular orbitals) and LUMO (lowest unoccupied molecular orbitals) (Brabec et al. 2003; Lakowicz 2006; Kemp 1975). Let us take a few examples. C_2H_6 , C_2H_4 and C_2H_2 molecules have C–C, C

= C and C≡C bonds, respectively. Hybridization of C in C₂H₆, C₂H₄ and C₂H₂ molecules form sp³, sp² and sp, respectively. Benzene molecule is having 3 π-bonds and 6 σ-bonds in adjacent bonds to form 6 carbon atoms ring. In resonance, these 3 π-bonds form a ring inside 6 carbon atoms ring. Absorption band shifts to a longer wavelength with an increase of π- bonds conjugation in a series of organic molecules and thus, the wavelength of its emission moves longer. This trend is seen in benzene, naphthalene, and anthracene. Similarly, ZnO absorbs light in 300–360 nm and its emission spectrum can produce a peak at 380 nm (corresponding to absorption edge) along with a broad emission band in 400–600 nm (Singh et al. 2009a; Ghosh et al. 2011).

There is another process known as quantum cutting, which is also a part of frequency down-conversion.

2.2.1.2 Quantum Cutting

Quantum cutting (QC) is one type of down-conversion (DC) process in which two or more low-energy photons are produced from a high-energy photon absorption (Yadav and Ningthoujam 2021; Mir et al. 2020; Zou et al. 2016; Zhang and Huang 2010). The QC process is observed in both singly rare-earth (RE) doped materials as well as in doubly or triply doped rare-earth doped materials. Here, energy transfer occurs through cooperative energy transfer (CET) process. In most cases, emitted light due to QC is observed in NIR range, whereas excitation wavelength is chosen in UV or visible light. In some cases, QC is observed in visible range upon excitation in vacuum UV region. The light emitted due to down-conversion or down-shifting in visible range is linear-dependent on excitation intensity, whereas the light emitted due to QC in NIR range is non-linear-dependent on excitation intensity. Figure 2.2 shows the schematic diagrams of QC mechanism for single ion and double ions in various hosts.

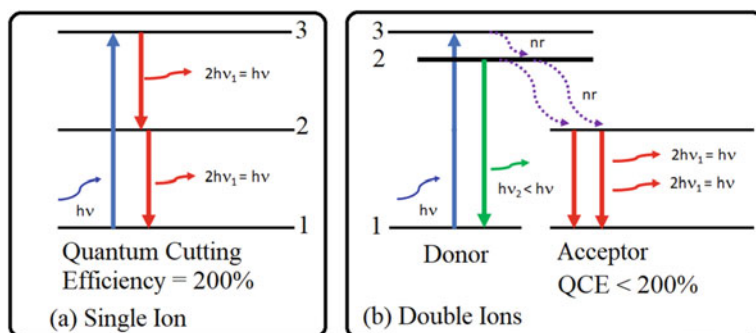
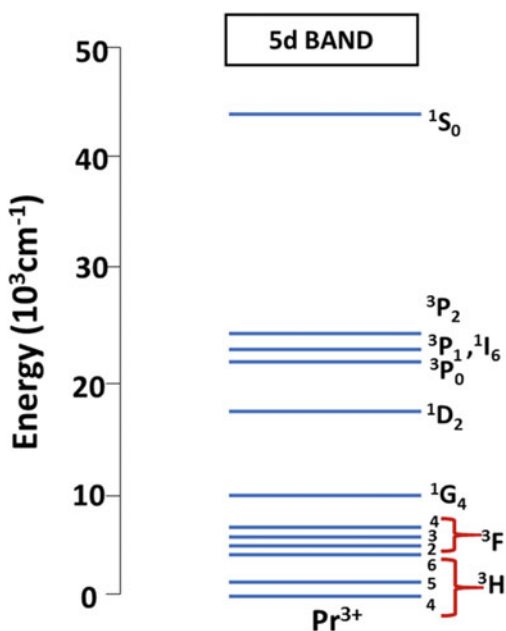


Fig. 2.2 Schematic diagram showing Quantum Cutting (QC) in single ion and double ions doped samples. Here, metastable energy levels help in getting QC

The first theoretical proposal to produce light with quantum yield (QY) more than 100% was reported in 1957 by Dexter (Dexter 1957). The transfer of energy from one sensitizer to two or more activators under different conditions can produce light with $QY > 100\%$. It was realized experimentally in Pr^{3+} doped LaF_3 , YF_3 and NaYF_4 in 1973 by a group of researchers from The Netherlands and USA (Sommerdijk et al. 1974; Piper et al. 1974). Upon excitation at 210 nm or 185 nm, the peak at 400–410 nm was observed. This transition corresponds to $^1\text{S}_0$ - $^3\text{P}_2$ (4f-4f transition of Pr^{3+}) and is related to quantum cutting (QC) process because half of 400–410 nm is 200–205 nm. Figure 2.3 shows the schematic energy level diagram of Pr^{3+} ($4f^2$ electrons) and 5d levels (Piper et al. 1974). In a weak crystal field environment, 5d level is above $^1\text{S}_0$. In such conditions, the emission peak at 400–410 nm is observed under 185 nm excitation (Fig. 2.4) (Piper et al. 1974). If the excitation is done at 213 nm, an emission peak at 400–410 nm is observed, but this emission peak could not be observed under 228 nm excitation (Fig. 2.5) (Sommerdijk et al. 1974). In a strong crystal field environment, 5d levels become below $^1\text{S}_0$. Here, 5d levels are split into t_{2g} and e_g levels. Then excited energy is transferred to 5d levels non-radiatively, and the transition from $^1\text{S}_0$ becomes weaker. This was observed in CaF_2 and oxide compounds doped with 1 at.% Pr^{3+} . Instead of this, other transitions above 450 nm occur. If energy of excitation is less than $^1\text{S}_0$ level, other 4f-4f transitions above 450 nm occur.

In general, the materials having quantum cutting properties contain rare-earth ions, which may act as a part of host or dopants. Systems are Tb^{3+} - Yb^{3+} , Tm^{3+} - Yb^{3+} , Pr^{3+} - Yb^{3+} , Ce^{3+} - Yb^{3+} , Er^{3+} - Yb^{3+} , Ce^{3+} - Tb^{3+} - Yb^{3+} , and Gd^{3+} - Eu^{3+} , etc.

Fig. 2.3 Schematic energy level diagram for Pr^{3+} showing the positions of $4f^2$ levels as well as 4f-5d transition but the position of 5d level is dependent on the strength of ligand neighbouring to Pr^{3+} ion. It is redrawn and adapted from Elsevier Publisher (Piper et al. 1974)



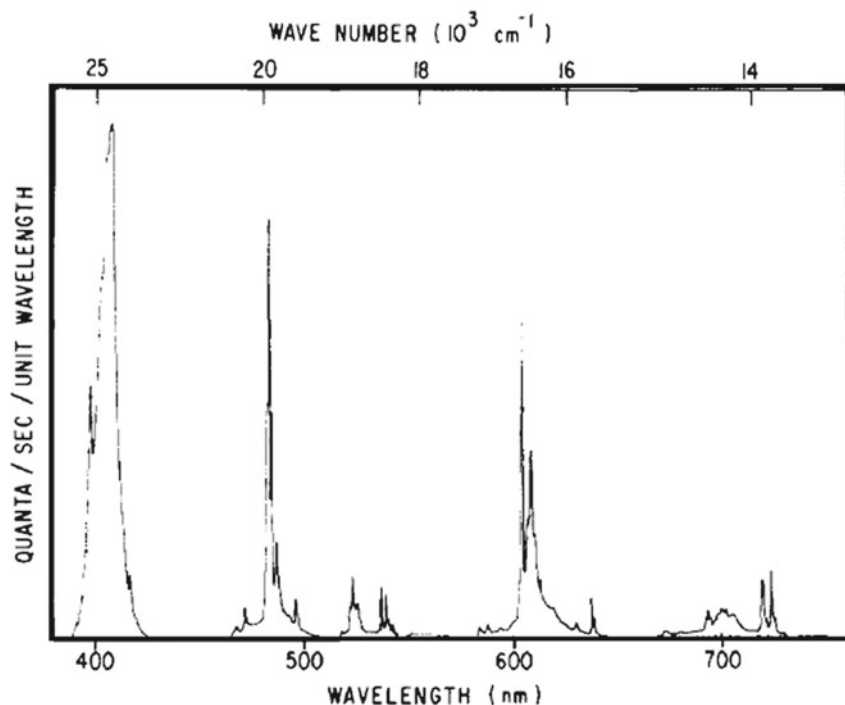


Fig. 2.4 Photoluminescence spectrum for YF₃: 0.1 at.% Pr³⁺ under excitation at 185 nm. It is reproduced with permission from Elsevier Publisher (Piper et al. 1974)

(Yadav and Ningthoujam 2021; Mir et al. 2020; Zou et al. 2016; Zhang and Huang 2010; Huang and Zhang 2010). Nowadays, other ions (from d or p block elements) are added as sensitizers (Bi³⁺–Yb³⁺). It is to be remembered that f electrons can have many fixed energy levels at different excited states. From this, possibility of many emission peaks can occur from UV to visible to NIR regions depending on the availability of levels. Photon-cascade emission phenomena can occur through frequency down and up-conversion processes.

In vacuum ultraviolet (VUV) excitations, visible emission peaks in 560–640 nm (maximum peak at 590 nm) are observed from Gd³⁺ doped LiYF₄ (singled ion) (Wegh et al. 1997). This is due to QC process. These transitions are assigned to ⁶G_j → ⁶P_j (Here j = spin–orbit coupling that can produce the Stark Splitting). Under VUV, electrons at ground state ⁸S_{7/2} go to the excited state ⁶G_j. Then excited electrons come to the lower energy levels such as ⁶D_j, ⁶I_j and ⁶P_j through radiative or non-radiative processes or mixing. Then radiative transition from ⁶G_j to ⁶P_j produces visible light. The transition from ⁶G_j to ⁸S_{7/2} at 205 nm, ⁶I_j to ⁸S_{7/2} at 275 nm and ⁶P_j to ⁸S_{7/2} at 310 nm can produce emission. These are explained in Figs. 2.6, 2.7 and 2.8 (Wegh et al. 1997).

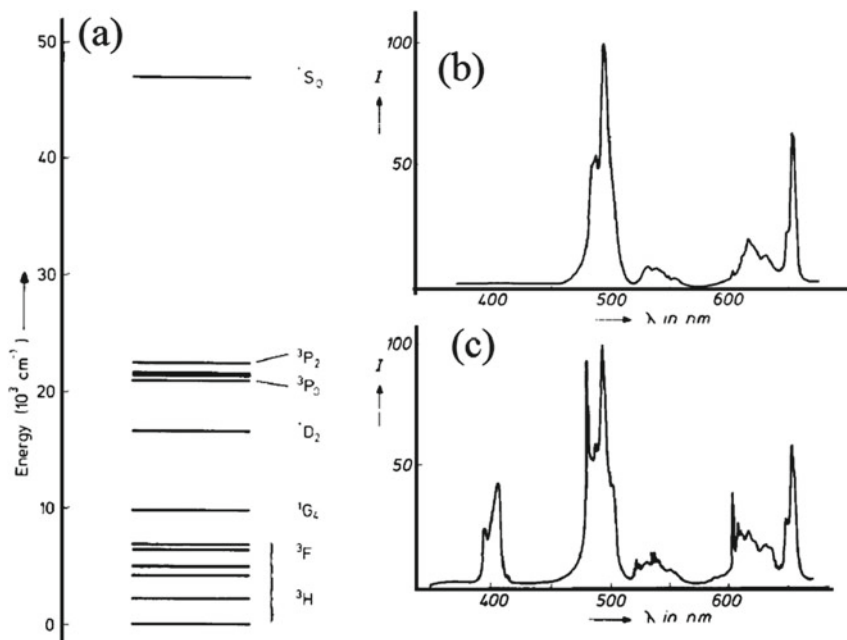
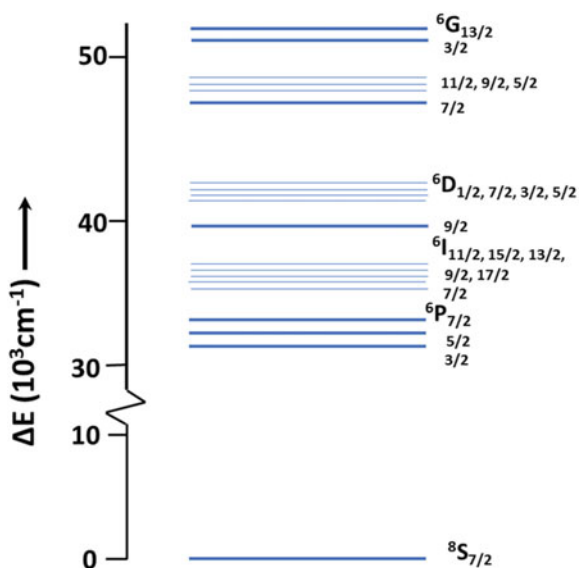


Fig. 2.5 a 4f energy level scheme of Pr³⁺. Photoluminescence spectrum for YF₃: 0.1 at.% Pr³⁺ after excitation at **b** 228.8 (Cd lamp) and **c** 213 nm (Zn lamp). It is reproduced with permission from Elsevier Publisher (Sommerdijk et al. 1974)

Fig. 2.6 Schematic energy level scheme in the 0–50,000 cm⁻¹ range for Gd³⁺ in fluoride lattice. It is redrawn and adapted from American Physical Society (APS) Publisher (Wegh et al. 1997)



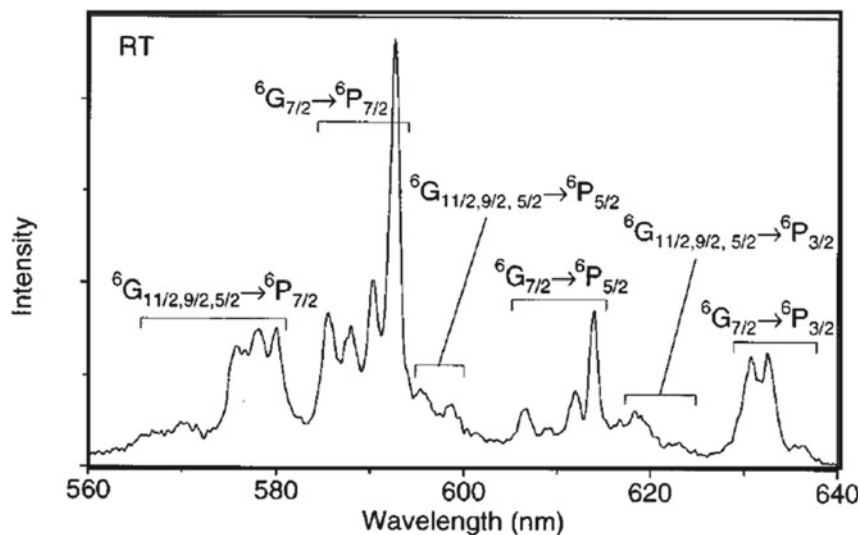


Fig. 2.7 ${}^6G_j \rightarrow {}^6P_j$ emission spectrum of $\text{LiYF}_4: 5 \text{ at.}\% \text{ Gd}^{3+}$ upon excitation at 202.1 nm (${}^8S_{7/2} \rightarrow {}^6G_j$) at 300 K . It is reproduced with permission from American Physical Society (APS) Publisher (Wegh et al. 1997)

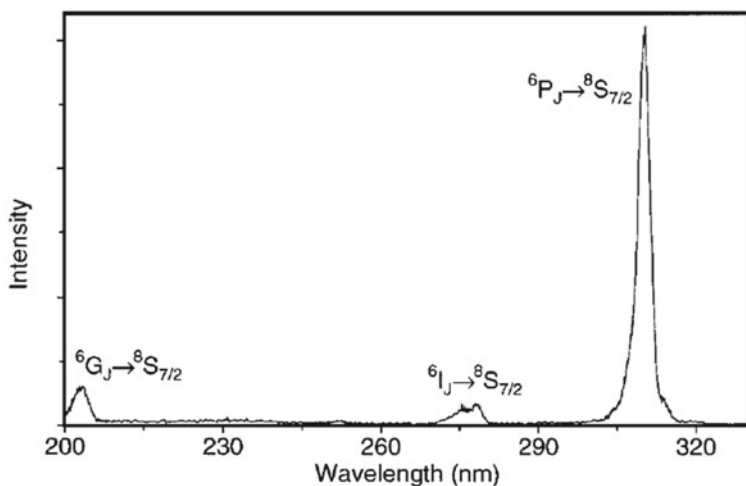


Fig. 2.8 UV emission spectrum of $\text{LiYF}_4:5 \text{ at.}\% \text{ Gd}^{3+}$ upon excitation at 194.7 nm (${}^8S_{7/2} \rightarrow {}^6G_{13/2}$) at 300 K . It is reproduced with permission from American Physical Society (APS) Publisher (Wegh et al. 1997)

Visible quantum cutting is observed in $\text{LiGdF}_4:\text{Eu}^{3+}$ through down-conversion. Figure 2.9 shows schematic energy levels for two lanthanide ions (1 & 2 types hypothetically), which can have an energy transfer process for down-conversion process (Wegh et al. 1999). Ion 1 can undergo absorption and emission in one case and in another case, its energy can be transferred to ion 2. (I) A single ion (1) exhibits quantum cutting (QC) through the successive emission of two visible photons after absorption of UV light. (II) Quantum cutting through a two-step energy transfer. First step: Energy transfer from ion 1 to ion 2 takes place as a part of the excitation energy by cross-relaxation. Then, ion 2 comes back to the ground state with the emission of one photon in the visible range. Remaining energy of ion 1 is in an excited state and can transfer to a second ion of type 2. From a second ion of type 2, emission of a photon in the visible spectral region can occur. Here, a quantum efficiency of 200% is expected. (III and IV) Other possible QC processes: There is only one energy transfer process from ion 1 to ion 2, which can generate two photons in the visible range.

Figure 2.10 shows the energy level diagram of the $\text{Gd}^{3+}-\text{Eu}^{3+}$ system, showing the possibility of visible quantum cutting by a two-step energy transfer from Gd^{3+} to Eu^{3+} (Wegh et al. 1999). In $\text{Gd}^{3+}-\text{Eu}^{3+}$ system (Eu^{3+} doped LiGdF_4), emission intensity coming out from ${}^5\text{D}_0$ is more than a factor of 2 stronger for excitation at 202 nm (${}^6\text{G}_j$) than that for excitation at 273 nm (${}^6\text{I}_j$). This is due to QC effect. In the case of excitation at 202 nm, excited electrons go to the higher excited state of Gd^{2+} (${}^6\text{G}_j$)

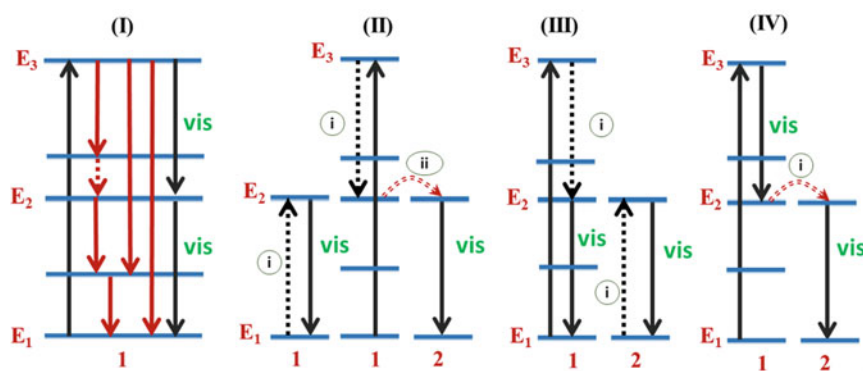


Fig. 2.9 Schematic energy level diagrams for two types of lanthanide ions (1 and 2), which can show possibility for the quantum cutting processes through frequency down-conversion. Possible way (I): A single ion (1) exhibits quantum cutting (QC) through the successive emission of two visible photons after absorption of UV light. Way (II): Quantum cutting through a two-step energy transfer. First step: Energy transfer from ion 1 to ion 2 takes place as a part of the excitation energy by cross-relaxation. Then, ion 2 comes back to the ground state with the emission of one photon in the visible range. Remaining energy of ion 1 is in an excited state and can transfer to a second ion of type 2. From a second ion of type 2, emission of a photon in the visible spectral region can occur. Ways (III and IV): There is only one energy transfer process from ion 1 to ion 2, which can generate two photons in the visible range. It is redrawn and adapted from the American Association for the Advancement of Science (AAAS) Publisher (Wegh et al. 1999)

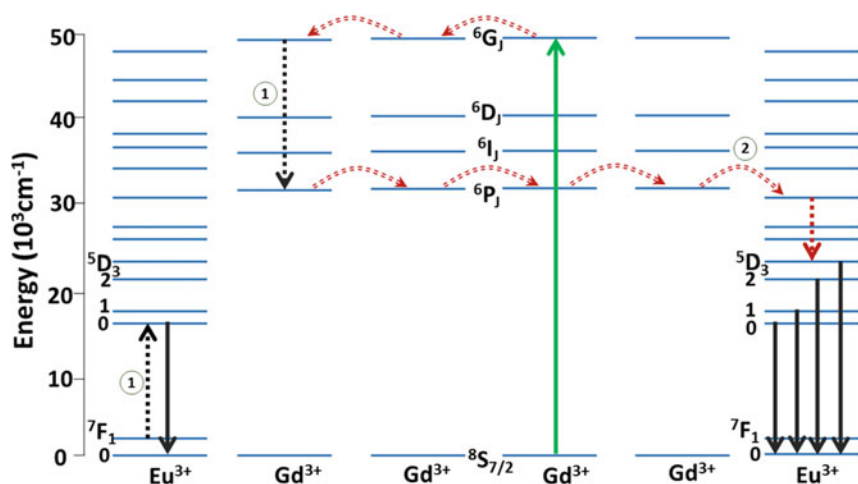


Fig. 2.10 Schematic diagram illustrating energy levels of the Gd^{3+} - Eu^{3+} pair with the possibility of quantum cutting in the visible range through a two-step energy transfer from Gd^{3+} to Eu^{3+} . Here, Gd^{3+} ions absorb light of a single photon in the UV region and it produces visible light. It is redrawn and adapted from the American Association for the Advancement of Science (AAAS) Publisher (Wegh et al. 1999)

and come to a lower energy level (${}^6\text{P}_j$). During this transition, electrons in ground state of Eu^{3+} (${}^7\text{F}_j$) go to excited state (${}^5\text{D}_0$). This is known as cross-relaxation. Then visible red emission from ${}^5\text{D}_0$ level occurs. Simultaneously, the remaining excited electrons at ${}^6\text{P}_j$ of Gd^{3+} are transferred or migrated to the excited states of ${}^5\text{D}_j$ of Eu^{3+} . The visible red emission occurs. In this way, two photons (left from Eu^{3+} due to cross-relaxation and right from Eu^{3+} due to energy transfer or migration in Fig. 2.10) in visible red region occur. Here, one Gd^{3+} ion acts as sensitizer and 2 Eu^{3+} ions act as activator. In case of excitation at 273 nm (${}^6\text{I}_j$), excited electrons go to the higher excited state of Gd^{3+} (${}^6\text{I}_j$) and come to a lower energy level (${}^6\text{P}_j$) through non-radiative process. Then excited electrons at ${}^6\text{P}_j$ of Gd^{3+} are transferred or migrated to excited states of ${}^5\text{D}_j$ of Eu^{3+} . The visible red emission occurs. In this way, one photon in visible red emission occurs.

In Yb^{3+} - Tm^{3+} system (YPO_4 : Yb-Tm), an emission peak of 647 nm due to Tm^{3+} occurs after excitation at 475 nm excitation (direct excitation of Tm^{3+}) (Xie et al. 2009). When amount of Yb^{3+} increases, emission intensity of Tm^{3+} decreases, whereas the emission intensity due to Yb^{3+} in 970–1000 nm increases. There is an energy transfer from Tm^{4+} to Yb^{3+} . This was supported by a decrease in the lifetime of 647 nm peak after addition of Yb^{3+} . This is explained by QC process because 2 times of 475 nm gives 950 nm, which is near to 970 nm. After phonon relaxation, emission occurs in 970–1000 nm. This is explained by Figs. 2.11 and 2.12 (Xie et al. 2009). This energy transfer process is cooperative energy transfer.

In case of Bi^{3+} - Yb^{3+} system (Gd_2O_3 : Bi-Yb), emission spectrum of Yb^{3+} in 900–1100 nm is observed after excitation through Bi^{3+} (320–390 nm) (Huang and Zhang

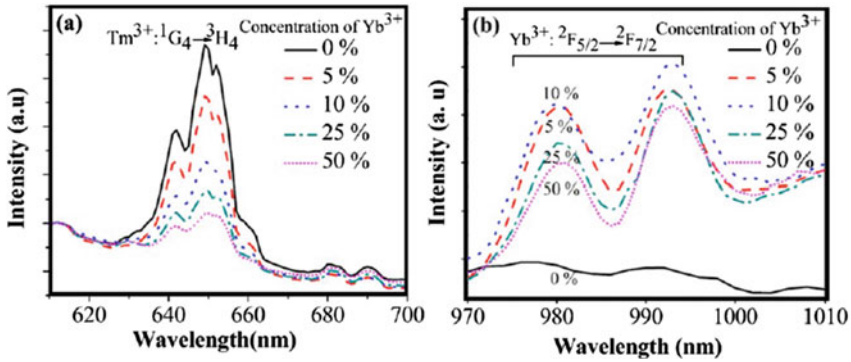


Fig. 2.11 Emission spectra of YPO₄: Yb-Tm after excitation at 475 nm: **a** emission spectra of Tm³⁺ in visible range and **b** emission spectra of Yb³⁺ in NIR range. It is reproduced with permission from American Institute of Physics (AIP) Publisher (Xie et al. 2009)

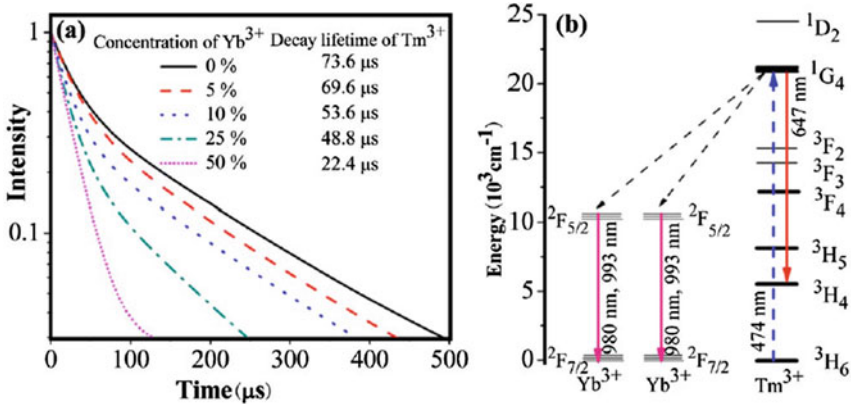


Fig. 2.12 **a** Decay profiles of the ¹G₄ → ³H₄ transition of Tm³⁺ at 647 nm and **b** schematic energy level diagram illustrating QC light in NIR region. It is reproduced with permission from American Institute of Physics (AIP) Publisher (Xie et al. 2009)

2010). Without Yb³⁺, emission in 400–700 nm occurs and this is due to the transition from ³P₁ excited state to ¹S₀ ground state of Bi³⁺. With increase of Yb³⁺ amount, emission intensity of Bi³⁺ decreases, whereas emission intensity of Yb³⁺ increases. This is related to QC effect. Here, the lifetime of Bi³⁺ after excitation at 347 nm decreases with an increase of Yb³⁺ amount. This transfer of energy from Bi³⁺ to Yb³⁺ is referred as cooperative energy transfer (CET). The schematic diagram as well as the associated emission and decay processes is shown in Figs. 2.13, 2.14 and 2.15 (Huang and Zhang 2010).

The energy transfer efficiency (ETE, η_{ETE}) is calculated using the following:

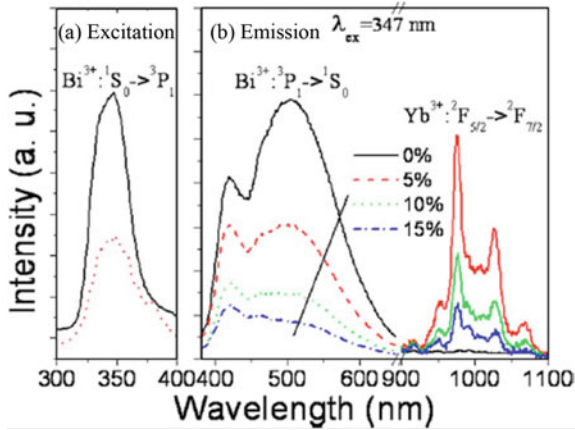


Fig. 2.13 a PL excitation spectra of $(\text{Gd}_{0.99}\text{Bi}_{0.01})_2\text{O}_3$ sample (solid line) monitored emission at 506 nm (Bi^{3+} emission peak) and $(\text{Gd}_{0.94}\text{Yb}_{0.05}\text{Bi}_{0.01})_2\text{O}_3$ sample (dashed line) monitored emission at 977 nm. b PL spectra of $(\text{Gd}_{0.99-x}\text{Yb}_x\text{Bi}_{0.01})_2\text{O}_3$ samples in visible—NIR range after excitation at 347 nm (Bi^{3+} excitation/absorption peak). It is reproduced with permission from American Institute of Physics (AIP) Publisher (Huang and Zhang 2010)

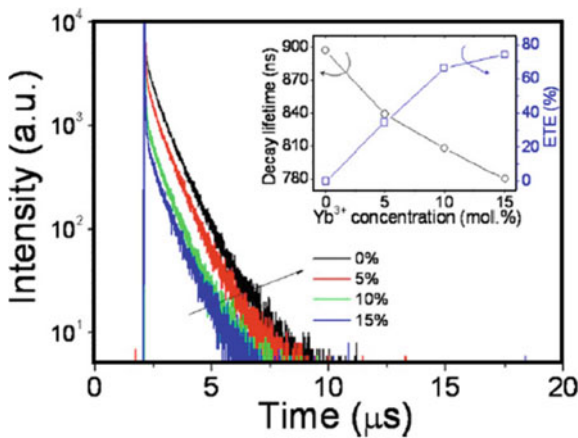


Fig. 2.14 Decay profiles of Bi^{3+} (${}^3\text{P}_1 \rightarrow {}^1\text{S}_0$) emission peak upon excitation at 347 nm in $(\text{Gd}_{0.99-x}\text{Yb}_x\text{Bi}_{0.01})_2\text{O}_3$ samples. Inset shows decay lifetime values and energy transfer efficiency from Bi^{3+} to Yb^{3+} at different amounts of Yb^{3+} . It is reproduced with permission from American Institute of Physics (AIP) Publisher (Huang and Zhang 2010)

$$\eta_{ETE} = \eta_{x\%Yb} = 1 - \frac{\int I_{x\%Yb} dt}{\int I_{0\%Yb} dt} \tag{2.1}$$

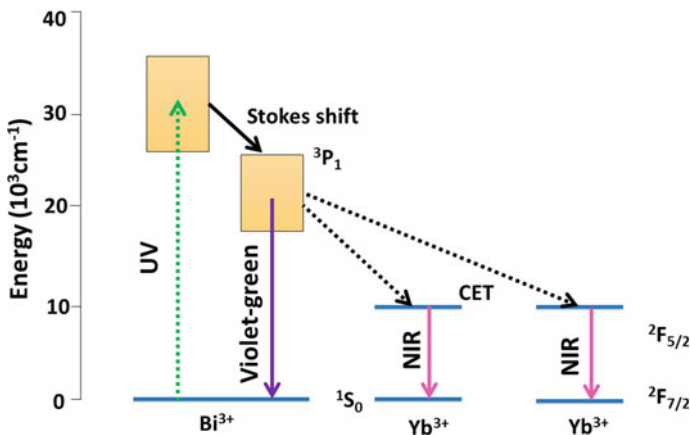


Fig. 2.15 Schematic diagram illustrating energy levels of ions (Bi^{3+} and Yb^{3+}) in Gd_2O_3 host. CET process for QC luminescence in NIR range under UV excitation is provided. It is redrawn and adapted from American Institute of Physics Publisher (Huang and Zhang 2010)

Here, $\int I_{x\%Yb} dt$ and $\int I_{0\%Yb} dt$ are luminescence intensities of sensitizer (Bi^{3+}) in the presence of activator (Yb^{3+}) and of sensitizer (Bi^{3+}) in the absence of activator (Yb^{3+}), respectively.

The quantum efficiency (QE, η_{QE}) of activator (Yb^{3+}) is calculated by the following relation:

$$\eta_{QE} = \eta_{Bi}(1 - \eta_{ETE}) + 2\eta_{Yb}\eta_{ETE} \quad (2.2)$$

where, η_{Bi} and η_{Yb} are the quantum efficiencies of Bi^{3+} and Yb^{3+} , respectively. If their values become 100% or 1.0, the equation (2.2) can be written as

$$\eta_{QE} = (1 - \eta_{ETE}) + 2\eta_{ETE} \quad (2.3)$$

Lanthanide doping in metal halide perovskite nanocrystals ($\text{CsPbX}_3:\text{Ln}^{3+}$ ($X = \text{Cl}, \text{Br}, \text{I}$)) also exhibit quantum cutting luminescence (Mir et al. 2020). Near-infrared quantum cutting long persistent luminescence (NQPL) has been observed in phosphor $\text{Ca}_2\text{Ga}_2\text{GeO}_7:\text{Pr}^{3+}, \text{Yb}^{3+}$ (Zou et al. 2016). Many examples of quantum cutting can be found in Ln doped oxides and fluorides (Zhang and Huang 2010).

2.2.2 Frequency Up-Conversion Luminescence

In case of up-conversion luminescence, excitation energy or frequency is less than that of emission ($E_{em} > E_{exc}$ or $\nu_{em} > \nu_{exc}$) (Yadav and Ningthoujam 2021; Ningthoujam et al. 2022; Auzel 2004). It means that wavelength of excitation is more than that of

emission ($\lambda_{em} < \lambda_{exc}$). Figure 2.1b shows the up-conversion process schematically. At initial stage, an electron at the ground state goes to the excited state ($E_0 \rightarrow E_1$) by absorption of energy (preferably laser source) with decay lifetimes of a few microseconds. Absorption takes place within 10^{-15} s. Before coming down to the ground state, excited electron at E_1 is hit by another electron, which absorbs energy (if continuous wave laser is used). Now, excited electron at E_1 jumps to higher excited level E_2 ($E_1 \rightarrow E_2$). From higher excited level (E_2), electron comes back to the ground state (E_0). However, its emission energy is more than that of absorbed energy. Sometimes, if excited energy levels have metastable states (like ladder like states in case of lanthanide ions), excited electron can jump to higher energy states ($E_2 \rightarrow E_3, E_3 \rightarrow E_4, \dots$) by multi-photon absorption process. Various energy transfer processes can take place within neighbouring ions.

Different types of up-conversion processes can take place depending on materials, excitation source and condition (Fig. 2.16) (Yadav and Ningthoujam 2021; Ningthoujam et al. 2022; Auzel 2004). In most cases, resonance type absorption occurs. There is another process known as photon avalanche, which is similar to up-conversion process, but excitation intensity is more than the critical value as well as non-resonance type absorption occurs in high concentration of activators/dopants present in a host.

The frequency up-conversion mechanisms are useful in the following applications such as (a) infrared (IR) quantum counter detectors, (b) security ink, (c) temperature sensors, (d) three different colour emitting phosphors, (e) compact visible or (f) ultraviolet (UV) solid state lasers, (g) imaging through NIR excitations, (h) energy conservations, (i) light induced isomerism in organic molecules, (j) MRI contrast agents, (k) multi-utility at different excitation sources such UV, Visible, NIR lights, (l) deep tissue photothermal therapy, (m) photodynamic therapy, etc.

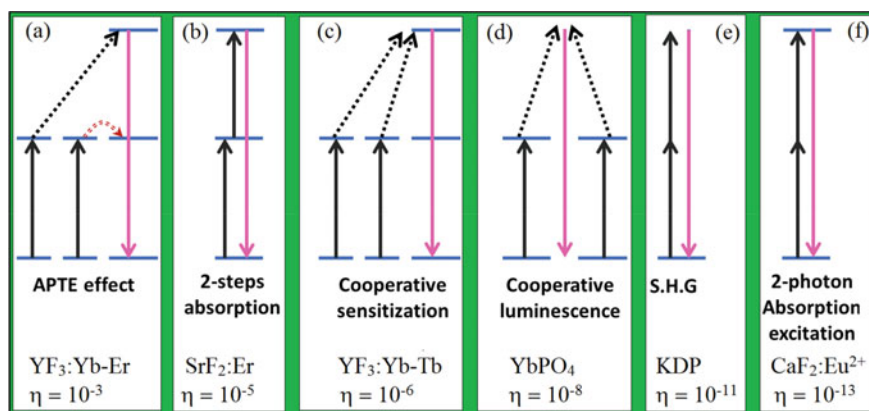


Fig. 2.16 Schematic diagram illustrating various 2-photon up-conversion processes observed in different systems. Here, relative efficiency in respective hosts is provided. It is redrawn and adapted from ACS Publisher (Auzel 2004)

2.2.2.1 Organic Based Frequency Up-Converters

Organic based frequency up-converters have been produced. Here sensitizer-activator combination can bring a light in UV to visible by absorbing suitable light in the whole solar spectrum. This will be useful in light energy harvesting. Here, triplet–triplet annihilation (TTA) mechanism is involved (Singh-Rachford and Castellano 2010). The sensitizer absorbs light from the ground state (GS = $^1S_0^s$ to the first excited state ($^1ES^* = ^1S_1^s$). This excited energy is transferred to its triplet state ($^3ES^* = ^3T_1^s$) through inter-system-crossing (ISC). The energy of $^3T_1^s$ is absorbed by the triplet state ($^3Acceptor^* = ^3T_1^a$) of activator through triplet–triplet energy transfer (TTET). At the same time, another molecule of activator has a similar TTET since a continuous source of excitation is provided. Combined 2 triplets of activators ($^3T_1^a$ – $^3T_1^a$) produce light, which is absorbed by activator in such a way that the electrons in ground state of acceptor/activator go to the singlet excited state ($^1Acceptor^*$, i.e., from GS ($^1S_0^a$) to ES ($^1S_1^a$)). This process is known as annihilation (loss or extinction or destruction) or triplet–triplet annihilation. Finally, light is produced from the excited state of activator ($^1S_1^a$) to ground state ($^1S_0^a$). The frequency of light produced is more than that of absorption by sensitizer. It is shown in Fig. 2.17 (Singh-Rachford and Castellano 2010). To meet the above condition, the energy gap of sensitizer phosphor is less than that of activator phosphor. The triplet excited energy of sensitizer is slightly more than that of triplet excited energy of activator. Energy of 2 triplet excited states of 2 activators is equal to or a slightly more than that of singlet excited state of activator. The difference will be provided by phonon relaxation. It is to be noted that triplet excited state has a relatively longer lifetime (μ s to ms), which helps in triplet–triplet annihilation. Absorption of light by sensitizer takes place within 10^{-15} s.

In general, metal complex molecules having metal-to-ligand charge transfer (MLCT) is used as sensitizer. Metals are heavy noble metals such as Pd, Pt and Ru. Ligands have π -conjugated aromatic rings such as porphyrins and phthalocyanines. Such central metal ion in porphyrins enhances the spin–orbit coupling, which produces efficiency of unity for singlet–triplet intersystem crossing (ISC) (Singh-Rachford and Castellano 2010).

At 450 nm laser excitation, $[Ru(dmb)_2(bpy-An)]^{2+}$ in CH_3CN medium or solution exhibits the up-converted delayed singlet anthracene fluorescence through the bimolecular triplet–triplet annihilation (Fig. 2.18) (Kozlov and Castellano 2004). Excitation wavelength at 450 nm is related to MLCT. Emission occurs UV to visible range. Here, dmb is 4,4'-dimethyl-2,2'-bipyridine. bpy-An is 4-methyl-4'-(9-anthrylethyl)-2,2'-bipyridine. Laser power dependent emission studies show 2 photon absorption processes. Interestingly, solution having equal molar concentration of $[Ru(bpy)_3]^{2+}$ and anthracene (3.5×10^{-5} M) gives threefold enhancement in up-converted emission as compared to $[Ru(dmb)_2(bpy-An)]^{2+}$. It is suggested that intermolecular interaction (non-covalent interaction) is a better up-converted process as compared to that of intramolecular interaction (covalent interaction).

Without anthracene, $[Ru(bpy)_3]^{2+}$ alone does not produce up-converted emission instead, it produces down-converted emission after excitation at 450 nm. The

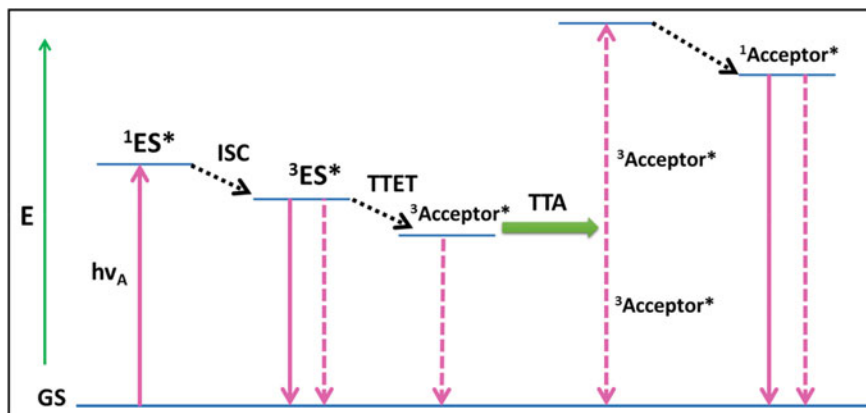


Fig. 2.17 Schematic diagram showing the up-conversion processes from the triplet state of the sensitizer molecule and the triplet state of the acceptor molecule and it leads to the singlet luminescence at higher energy. GS: ground state. ISC: intersystem crossing. ES: excited state. TTA: triplet–triplet annihilation and TTET: triplet–triplet energy transfer. Symbols “1” and “3” indicate the singlet and triplet states, respectively. It is redrawn and adapted from Elsevier Publisher (Singh-Rachford and Castellano 2010)

triplet excited state to singlet ground state transition (emission) occurs at 610 nm in CH_3CN solution and its lifetime is 920 ns. Laser power dependent emission studies show 1 photon absorption process. Anthracene alone does not produce up-converted emission after excitation at 450 nm. Chemical structures of $[\text{Ru}(\text{dmb})_2(\text{bpy}-\text{An})]^{2+}$, $[\text{Ru}(\text{bpy})_3]^{2+}$ and anthracene are shown here (Fig. 2.19) (Kozlov and Castellano 2004). Figure 2.20 shows the digital photo of up-converted light (blue) after excitation at the green light (laser at 532 nm) from the solution containing $[\text{Ru}(\text{dmb})_3]^{2+}$ and 9, 10-diphenyl-anthracene in CH_3CN solvent (Singh-Rachford and Castellano 2010).

2.2.2.2 Transition Metal Ions (d^{n+}) Based Frequency Up-Converters

Transition metal ions (TM = 3d, 4d, 5d) containing parent compounds or doped to other hosts have shown frequency up-converters (Ye et al. 2016). TM ions are Mn^{2+} , Cr^{3+} , Re^{4+} , V^{3+} , Mo^{3+} , Ni^{2+} , and Ti^{2+} , etc. However, they are extensively investigated at cryogenic temperatures except for Mn^{2+} and Cr^{3+} ions. This is due to a large influence from the electron–phonon coupling effect for d electrons of TM ions as compared to f electrons of Ln^{3+} ions. Also, there are large energy gaps between the ground state (${}^6\text{A}_1$ (Mn^{2+}) or ${}^4\text{A}_2$ (Cr^{3+})) and its first excited states (i.e., emitting levels = ${}^4\text{T}_1$ and ${}^4\text{T}_2$ (Mn^{2+}) or ${}^2\text{E}$ (Cr^{3+})) in cases of Mn^{2+} and Cr^{3+} ions. The energy gaps of about 10,000–20,000 cm^{-1} are observed and this reduces multi-phonon relaxation and thereby radiative emission at room temperature is observed. Figure 2.21

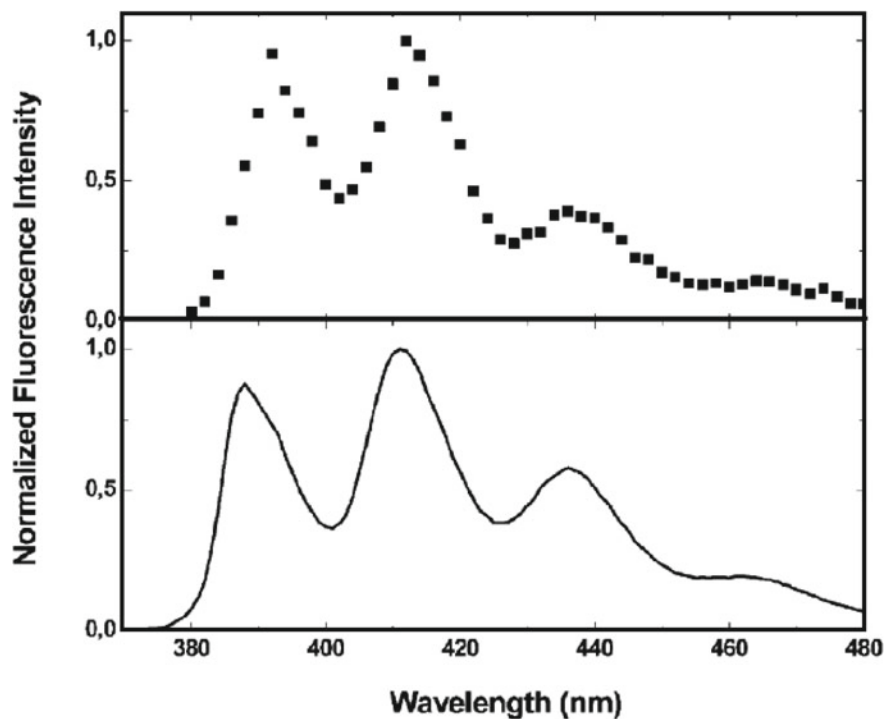


Fig. 2.18 Delayed luminescence spectrum of $[\text{Ru}(\text{dmb})_2(\text{bpy-An})]^{2+}$ (solid squares) in deaerated CH_3CN (3.5×10^{-5} M) measured 9 μs after a 450 nm excitation (power of 60 μJ laser pulse excitation). Residual luminescence from this (black line) using UV light 360 nm lamp excitation. It is reproduced with permission from RSC Publisher (Kozlov and Castellano 2004)

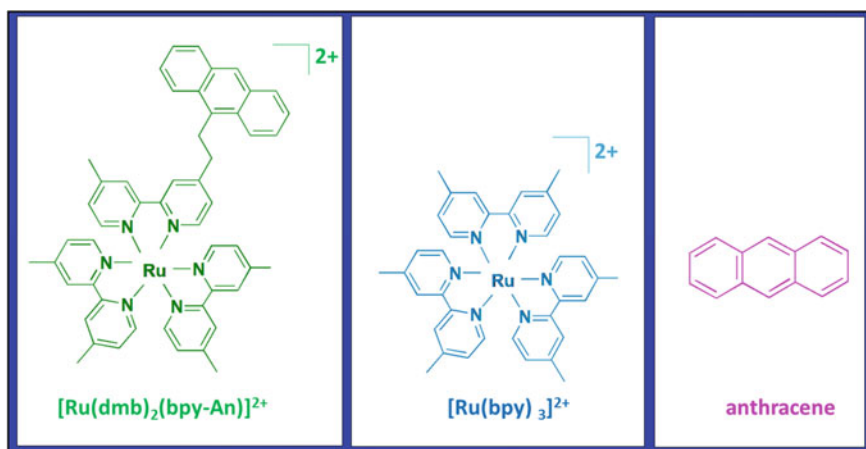


Fig. 2.19 Chemical structures of $[\text{Ru}(\text{dmb})_2(\text{bpy-An})]^{2+}$, $[\text{Ru}(\text{bpy})_3]^{2+}$ and anthracene

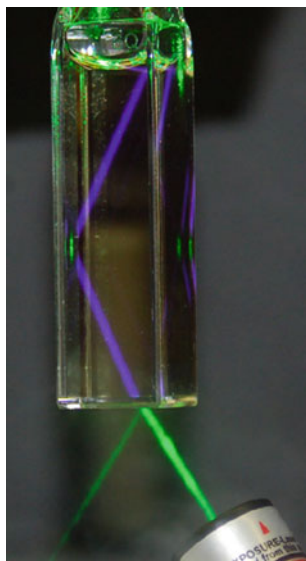


Fig. 2.20 Digital photograph of the up-converted light (blue) after excitation at the green light (laser at 532 nm) from solution containing $[\text{Ru}(\text{dmb})_3]^{2+}$ and 9, 10-diphenyl-anthracene in CH_3CN solvent. It is reproduced with permission from Elsevier Publisher (Singh-Rachford and Castellano 2010)

shows Tanabe-Sugano diagram of commonly used d^3 , d^5 and d^8 ions (Ye et al. 2016). These ions can show the room temperature up-conversion luminescence.

A broad yellow UC luminescence is observed at room temperature $\text{Ca}_3\text{Y}(\text{GaO})_3(\text{BO}_3)_4:\text{Yb}^{3+}\text{-Mn}^{2+}$ (CYGB: Yb-Mn) and CYGB: Yb phosphors upon 980 nm laser excitation (Fig. 2.22) (Xie et al. 2020). Two UC emission bands are observed at 503 and 600 nm. The 1st peak is related to the cooperative luminescence of Yb^{3+} pairs (CYGB: Yb) and 2nd peak is related to the transition of superexchange coupled $\text{Yb}^{3+} - \text{Mn}^{2+}$ pairs. There is no resonance energy transfer between coupled $\text{Yb}^{3+} - \text{Mn}^{2+}$ pairs. However, UC mechanism is explained on the basis of the ground state absorption (GSA) and followed by the excited state absorption (ESA) in this system (Fig. 2.23). Without Mn^{2+} , $\text{Ca}_3\text{Y}(\text{GaO})_3(\text{BO}_3)_4:\text{Yb}^{3+}$ shows emission at 503 nm due to emission from virtual level of Yb^{3+} by 2 photon absorption process (Fig. 2.23) (Xie et al. 2020).

2.2.2.3 Lanthanide Ions (Ln^{n+}) Based Frequency Up-Converters

Lanthanides include the elements having $4f^n$ electrons ($n = 1-14$) and comprise of 15 elements from lanthanum (atomic number 57) to lutetium (atomic number 71) (Ningthoujam et al. 2012). These have similar chemical properties with scandium (atomic number 21) and yttrium (atomic number 39), and are rarely available and also

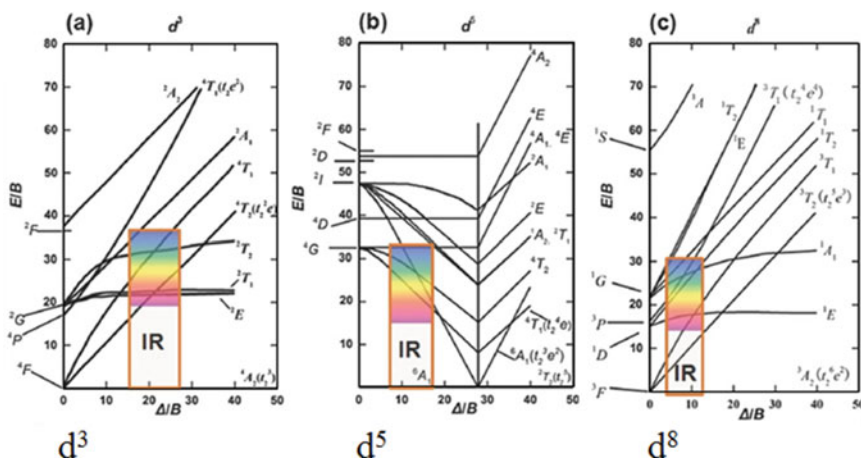


Fig. 2.21 Tanabe-Sugano diagram of a few 3d metal ions (d^3 , d^5 and d^8). Energy gap between the excited state and ground state is represented by the histogram. In this histogram, the coloured filled region denoted the energy levels located at visible range, whereas the empty region denoted the energy levels located at infrared (IR) range. It is reproduced under creative common & Wiley Online Library Publisher (Ye et al. 2016)

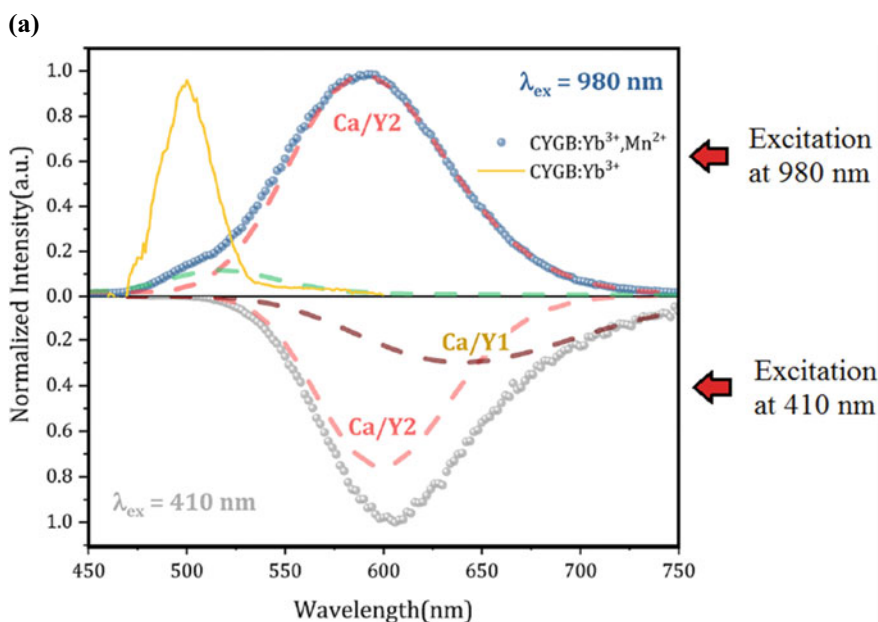
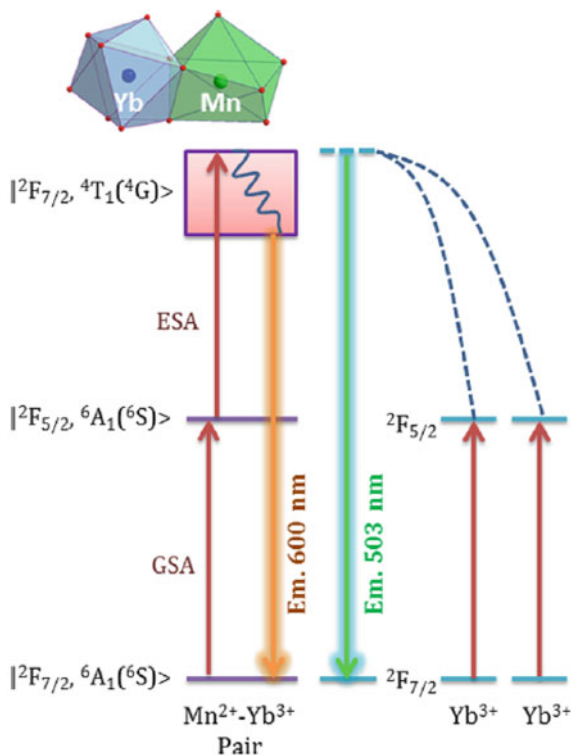


Fig. 2.22 Upper portion: normalized PL spectra (UC) for samples CYGB:0.01Yb³⁺, 0.45Mn²⁺ and CYGB:0.01Yb³⁺ after excitation at 980 nm. Lower portion: PL spectrum (DC) for sample CYGB:0.01Yb³⁺, 0.45Mn²⁺ after excitation at 410 nm. Gaussian fitting to spectrum is shown. It is reproduced with permission from ACS Publisher (Xie et al. 2020)

Fig. 2.23 Diagram showing proposed up-conversion of Yb^{3+} and Mn^{2+} in $\text{Ca}_3\text{Y}(\text{GaO})_3(\text{BO}_3)_4$: Yb^{3+} - Mn^{2+} phosphor under 980 nm excitation. It is reproduced with permission from ACS Publisher (Xie et al. 2020)



generally found in the same ore deposits as the lanthanides. These 17 elements are considered as the rare-earth elements. They have a stable oxidation state of +3 except in a few cases. Ce, Pr, Tb and Dy can have +3 or +4 depending on the oxidizing environment. Sm, Eu, Tm and Yb can exhibit +2 or +3 depending on the reducing environment. Nd can have +2 or +3 or +4. The ground state electronic configuration of Ln is $1s^2, 2s^2 2p^6, 3s^2 3p^6 3d^{10}, 4s^2 4p^6 4d^{10} 4f^{n \text{ or } n+1}, 5s^2 5p^6 5d^{1 \text{ or } 0}, 6s^2$ ($0 \leq n \leq 14$). La, Ce, Gd, and Lu have $[\text{Xe}] 4f^n, 5d^1, 6s^2$ and the remaining Ln elements have $[\text{Xe}] 4f^{n+1}, 6s^2$. In case of Ln^{3+} , the ground state electronic configuration is $1s^2, 2s^2 2p^6, 3s^2 3p^6 3d^{10}, 4s^2 4p^6 4d^{10} 4f^n, 5s^2 5p^6$ since 3 electrons from outer orbitals such as $6s^2$ and $5d^1$ or $4f^{n+1}$ are removed.

What types of electronic transition can take place in $4f^n$? $4f^n$ electron can go to higher excited states such as $4f$ or $5d$. The $4f^n$ to $4f^{n-1}5d^1$ transition occurs at vacuum UV ($\lambda_{\text{exc}} < 200 \text{ nm}$) or UV ($\lambda_{\text{exc}} = 200\text{--}300 \text{ nm}$) region. However, $4f^n$ to $4f^n$ transition occurs from UV to visible to NIR region. In general, $4f^n$ to $4f^n$ transition produces a sharp peak absorption, whereas, $4f^n$ to $4f^{n-1}5d^1$ transition produces a broad peak absorption because $5d^1$ degeneracy is lifted due to the crystal field from ligands present in around Ln^{3+} ion. $4f^n$ to $4f^n$ transition is forbidden and transition occurs due to relaxation such as mixing of orbitals or phonon relaxation or crystal field environment (Parchur and Ningthoujam 2012b; Srivastava et al. 2022). Ln^{3+}

ions with 4f electrons of $n = 1$ or 14 (Ce^{3+} or Lu^{3+}) do not undergo f-f transition in UV-visible-NIR range. Gd^{3+} with $n = 7$ (half field electrons) produces 4f-4f transition in UV region.

Due to the presence of metastable levels in higher excited states (due to spin-orbit coupling), many transitions (absorption and emissions) can take place. Such metastable levels can be used for up-converting process. Examples of up-converters are $NaYF_4: Er-Yb$, $NaYF_4: Tm-Yb$, $CaF_2: Er-Yb$, $LaF_3: Er-Yb$, etc. (Auzel 2004; Chen et al. 2004; Borse et al. 2022).

2.2.2.4 Actinide Ions (Ac^{n+}) Based Frequency Up-Converters

Actinide ions based frequency up-conversions are very less due to energy gaps between metastable levels are low and also association of f-d transition. In most cases, excited state absorption (ESA) up-conversion process is more as compared to that of sequential energy transfer or energy transfer (ETU) up-conversion process. Examples of Ac^{3+} ions doped samples are U^{4+} ($5f^2$) ions doped $ThCl_4$ or $ThBr_4$ and $ZnCl_2$ based glass, which have shown up-conversion luminescence (Auzel 2004; Karbowski et al. 2003; Shalav et al. 2007). Under 950 nm or 1170 nm excitation, green and red emission is observed and this up-conversion process is due to ESA because its emission intensity is linearly dependent on excitation laser power or its emission intensity is linearly dependent on the concentration of U^{4+} ions. $LaCl_3:U^{3+}$ ($5f^3$) shows the red emission under green laser excitation. Cm^{3+} ions doped samples have shown up-conversion luminescence.

2.2.2.5 Photon Avalanche

Photon avalanche (PA) is a process of frequency up-conversion in which a sudden increase in intensity of emitted light occurs when non-resonance type excitation is applied (Auzel 2004; Silva et al. 2020; Lee et al. 2021; Peng et al. 2022; Li et al. 2019). Generally, a high concentration of dopant (lanthanides) is associated in host so that cross-relaxation among dopant ions can occur. In such high concentration of dopant ions, when laser power of excitation source is provided above a critical value, huge cross-relaxation among dopant ions occurs and thereby, high intensity of frequency up-converted light is observed. It is a non-linear process and follows $I \propto P^n$ (I is intensity of converted light, P is power of excitation source and n is number of photons absorbed). Avalanched up-conversion phenomenon occurs $n > 10$; normal up-conversion process occurs when $n = 2-3$ and in between say $n = 4-7$, looping up-conversion occurs (Lee et al. 2021). In normal energy transfer up-conversion (sequential energy transfer, ETU), dopant concentration of activator ion is small (> 2 at.%, for example, $NaYF_4: 2$ at.%Er, 10 at.%Yb). Similarly, excited state absorption (ESA) up-conversion materials (for example $NaYF_4: Er$) also require less amount of activators (2 at.% Er). Otherwise, concentration quenching occurs. In ETU and ESA, the excitation wavelength should be close to the resonance with gap between

ground state energy and excited state energy, whereas the excitation wavelength of PA generally does not require resonance with gap between ground state energy and excited state energy, but it requires resonance with excited state intermediate levels (Lee et al. 2021; Levy et al. 2016).

For the first time, it was reported that when a LaCl_3 or LaBr_3 crystal doped with 4.8 at.% Pr^{3+} is exposed to simultaneous IR light at $4.5 \mu\text{m}$ and green CW laser, a red emission was obtained (Chivian et al. 1979). With increase of laser-pump power radiation, intensity of red emission increases. Above the critical power density of green CW laser $1.2\text{--}12.2 \text{ W/cm}^2$, red emission intensity is suddenly increased. Now, the intensity of red emission was independent of NIR light. This is known as Photon Avalanche. This was explained as follows: Pr^{3+} ion has the ground state energy level $^3\text{H}_4$ and metastable excited states start from $^3\text{H}_5$, $^3\text{H}_6$, $^3\text{F}_2$, $^3\text{F}_3$, $^3\text{F}_4$, $^1\text{G}_4$, $^1\text{D}_2$, $^3\text{P}_0$, $^3\text{P}_1$, $^1\text{I}_6$ to $^3\text{P}_2$. The energy levels are shown in Fig. 2.24 (Chivian et al. 1979).

When Pr^{3+} is exposed to IR at $4.5 \mu\text{m}$, $4f^2$ -electrons in ground state $^3\text{H}_4$ go to next higher excited state $^3\text{H}_5$. Further excitation with laser at green wavelength, excited electrons go to $^3\text{P}_1$ level (higher level). Possible emission transitions such as $^3\text{P}_1\text{--}^3\text{F}_2$, $^3\text{P}_0\text{--}^3\text{F}_2$, $^3\text{P}_0\text{--}^3\text{H}_6$ occur. This is one type of up-conversion process because of simultaneous two absorptions IR and green light. The intensity of red emitted light is linearly dependent on input power of IR or green light when input laser power is less than the critical value (P_c). At or above P_c , intensity of red light increases suddenly and shows non-linear property and without IR source, intensity of red light is very high (Fig. 2.25) (Chivian et al. 1979). This is explained by the non-radiative

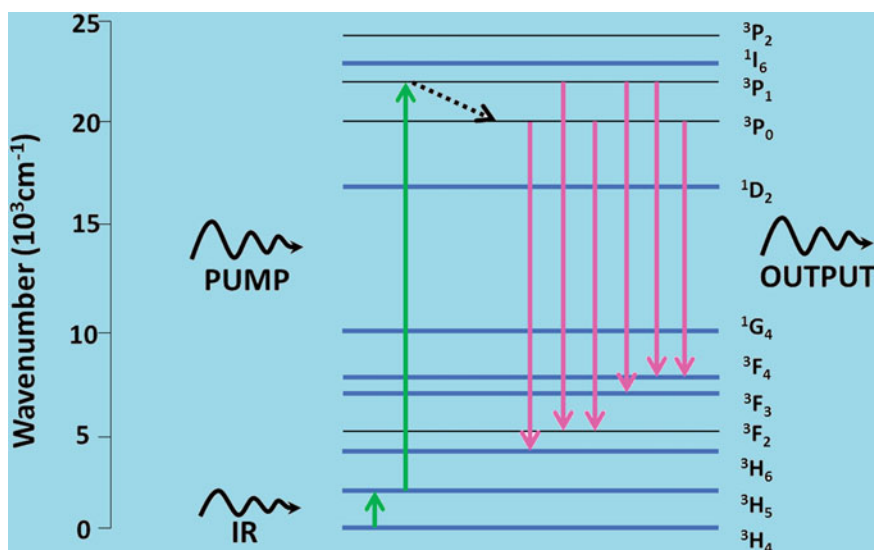


Fig. 2.24 Schematic energy levels of Pr^{3+} in LaCl_3 and LaBr_3 . Here, simultaneous IR light at $4.5 \mu\text{m}$ and green CW laser are provided. It is redrawn and adapted from AIP Publisher (Chivian et al. 1979)

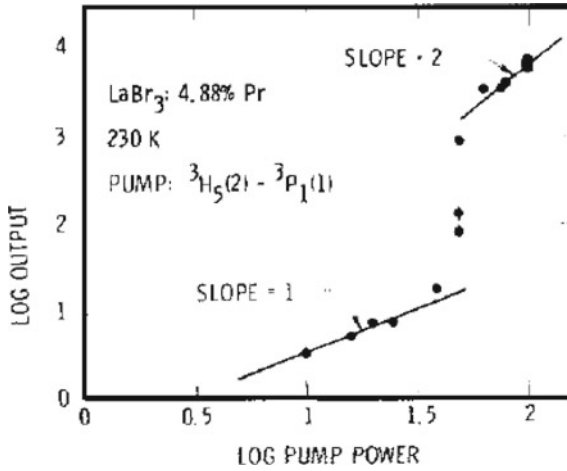


Fig. 2.25 Fluorescence output of Pr^{3+} versus incident pump power. The slope changes near to critical pump power density. It is reproduced with permission from AIP Publisher (Chivian et al. 1979)

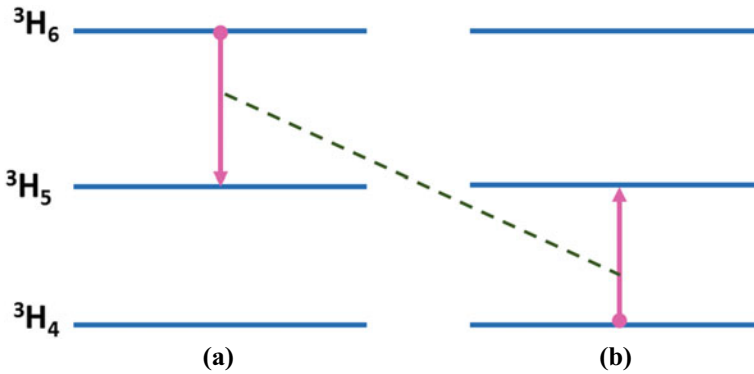


Fig. 2.26 Cross-relaxation among 2 Pr^{3+} ions **a** and **b**, which helps in population of excited electrons at ${}^3\text{H}_5$ level. It is redrawn and adapted from AIP Publisher (Chivian et al. 1979)

decay of ${}^3\text{H}_6$ to ${}^3\text{H}_5$, which is absorbed by another ion at ground state ${}^3\text{H}_4$ and goes to next higher energy state ${}^3\text{H}_5$. Such energy transfer is commonly known as cross-relaxation among two Pr^{3+} ions pair (Fig. 2.26) (Chivian et al. 1979). Above P_c , cross-relaxation process allows high population of electrons at ${}^3\text{H}_5$, which is further lifted to ${}^3\text{P}_1$ and then it emits light at red region (${}^3\text{H}_6$, ${}^3\text{F}_2$). Again cross-relaxation starts. This produces a loop or cycle or continuous process if the input green laser power is more than P_c .

Photon avalanche (PA) process is an unconventional pumping mechanism, which leads to a strong up-converted emission. Figure 2.27 shows the schematic way of

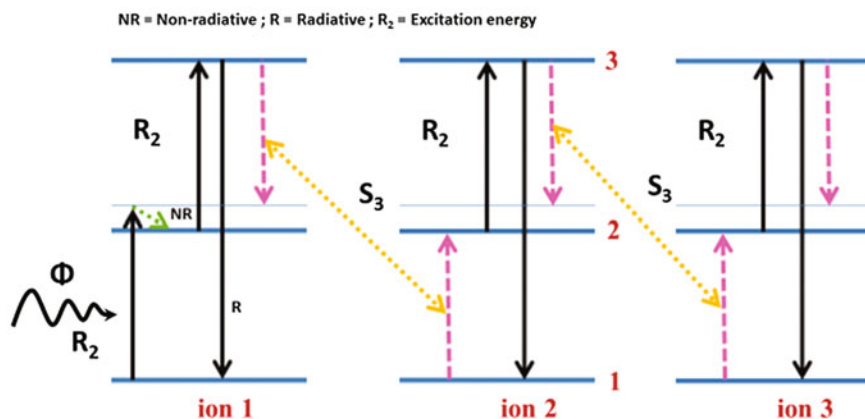


Fig. 2.27 Energy scheme for the simplest PA process in nearby 2 ions (1 and 2) and its energy transfer through cross-relaxation (S_3). It is redrawn and adapted from Ph. D. Thesis (Singh 2018)

PA process (Singh 2018). Pump photon is provided at metastable state (level 2) and excited electrons reach level 3. Some part of the excited electrons at level 3 comes back to level 2 and simultaneously electrons at the ground state go to the metastable level 2. This is known as cross-relaxation (CR) between 2 ions, which is shown by symbol (S_3). In this way, level 2 has a high population of excited electrons. Remaining part of the excited electrons at level 3 emits up-converted light and comes back to ground state level 1. Here, there is no ground state absorption (GSA) using a resonance energy between levels 1 and 2. Many theoretical models can be found in this review article and also many examples are provided (Joubert 1999).

2.3 Core@Shell Nanostructures

In terms of materials chemistry, the core-shell structure is a structure in which core particle is enclosed by a shell of different material/composition (Ningthoujam et al. 2022; Joshi et al. 2022a). Here, a core particle means a group of atoms that form either a perfect lattice or amorphous. Thickness may vary from 1 nm to a few microns. Different layers of shells can be created. It is not necessary to be nano-meter-size and can be micron size. Between core@shell, there will be an interface, which may be a secondary phase different from core and shell in terms of atomic ordering. Similarly, interface arises between layers of shells in a multilayer system. A core particle can have different shapes: sphere, cube, hexagon, prism, octahedron, disc, wire, rod, tube, sheet, star, tetra-pods, irregular, etc. If the size/thickness of at least one axis in x, y and z axis (3D) is nanometer, they can be considered in the nanomaterial category. Types of possible spherical core@shell structures are shown in Fig. 2.28 (Ningthoujam

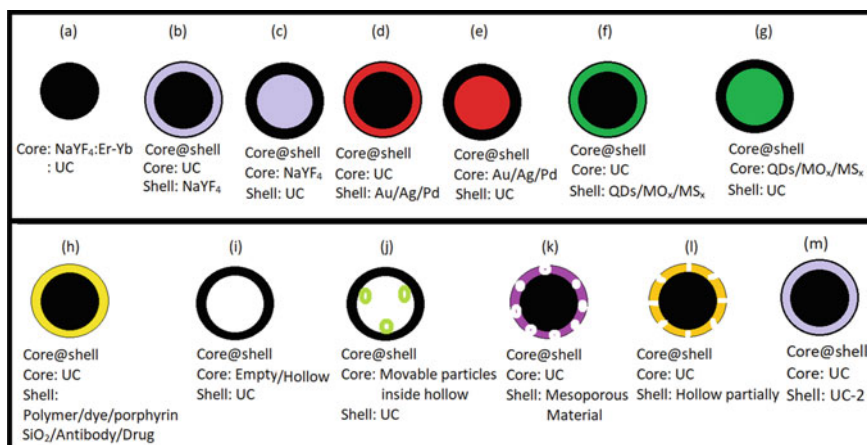


Fig. 2.28 Possible spherical Core@shell nanostructures. It is adapted from reference (Ningthoujam unpublished)

unpublished). In this study, up-converted nanomaterials are most considered. The symbol “UC” or “active UC” means that the nanoparticle is having active rare-earth ions or dopant ions, which are feasible for up-conversion process. Inactive means that there are no dopant ions. Similarly, other core@shell1@shell2, core@shell1@shell2@shell3 structures and so on can be possible (Figs. 2.29, 2.30, 2.31, 2.32, 2.33, 2.34 and 2.35) (Ningthoujam unpublished). Here, shell2 may be same as core material or a different material. In a similar way, shell3 may be same as shell1 or a different material. In nanosize range, it is easy to form core@shell formation kinetically. Nanoparticle is a group of atoms (100 to 10,000) that form a perfect lattice or amorphous phase in the nanosize range and at least one size is less than 50 nm in a particular axis (x, y or z axis). They are classified as 0D, 1D, 2D and 3D particles. Sometimes, many core particles can be enclosed by a particular shell. Such core particles can move on such hollow portions. If sufficient number of atoms is not available to make uniform shell thickness, it forms dispersed atoms over a particle. Interconnectivity between atoms of shell material may not be possible in such situation. In some cases, core particle is formed and same material is coated over to get different shapes and sizes (Oswald ripening route). So far, we assume that there is uniform thickness in the shell. To achieve such uniform thickness of shell, it requires special synthesis routes. In highly crystalline samples of similar crystal structure (hexagonal phase of β -NaYF₄, β -NaGdF₄ and doped samples), the layer-by-layer epitaxial growth can be performed. Sometimes, metal nanoparticles, SiO₂, mesoporous particles, polymers and any ligands can be used as core or shell (Johnson et al. 2012; Chaudhuri and Paria 2012; Mahdavi et al. 2020; Huseien 2023; Joshi et al. 2022b). In this system, it forms partial epitaxial growth or simply coating over the core. The formation of core@shell can be analysed by the following techniques (Ningthoujam et al. 2022).

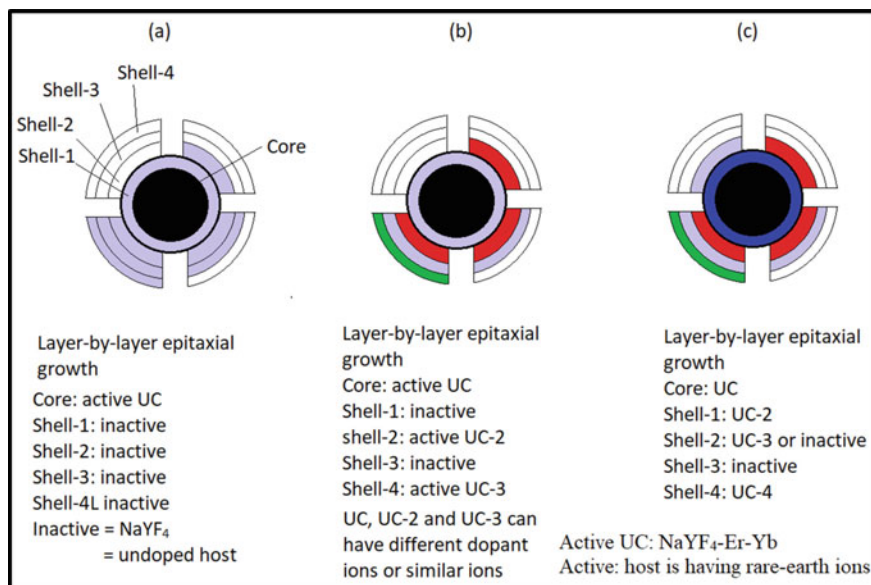


Fig. 2.29 Possible ways for layer-by-layer epitaxial growth of core and shell materials. Here, core is active up-converting material. It is adapted from reference (Ningthoujam unpublished)

1. Electron energy loss spectroscopy (**EELS**),
2. Line scanning energy dispersive x-ray spectroscopy (**EDAX**), but its resolution is less than that of **EELS**,
3. High-angle annular dark-field imaging (**HAADF**), which is a STEM technique,
4. Secondary ion mass spectrometry (**SIMS**), and
5. The x-ray absorption near edge spectroscopy (**XANES**).

2.3.1 Why Core@Shell Is Required?

What happens when core is coated with shell? The coating of core with other materials has many changes in nanosize particles such as suppression of surface dangling bonds or decrease of surface defects, band-gap manipulation for a particular application, easy to surface functionalization, stability, easy to dispersion in water or oil depending on the presence of surface functional groups, controlled release of drug loaded in core, reduction in consumption of precious core material, targeted therapy, improvement in diagnosis and therapy due to proper coating, manipulation of energy transfer or migration or concentration quenching or electron transfer in luminescence, manipulation in magnetic properties, change in catalytic properties, change in dielectric properties, changes in magnetoresistance, and so on (Ningthoujam et al. 2022; Joshi et al. 2021, 2022a, b; Auzel 2004; Ningthoujam unpublished; Johnson et al. 2012; Chaudhuri and Paria 2012; Mahdavi et al. 2020; Huseien 2023). In d- or f- ions doped core, it is assumed that ions are distributed homogenously in the

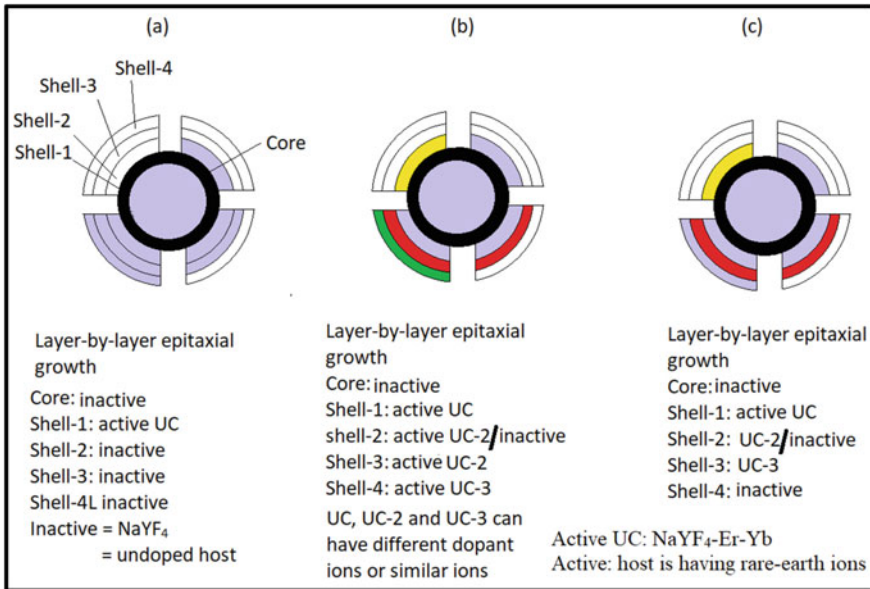


Fig. 2.30 Possible ways for layer-by-layer epitaxial growth of core and shell materials. Here, core is inactive material or undoped host material. It is adapted from reference (Ningthoujam unpublished)

core host lattice. This can be referred as homogenous system. When core is covered with undoped shell or doped shell and further coated with different shells, ions are no longer homogenous in the system (core@shell, core@shell1@shell2, core@shell1@shell2@shell3, etc.). This can be referred as heterogenous system in terms of distribution of d- or f- ions in the system. In homogenous system, concentration quenching due to high doping of d- or f- ions in luminescence is found. However, heterogenous system has unique properties, which are different from core properties. Even high concentrations of dopants can increase luminescence intensity. Mechanisms of energy transfer, energy migration, energy trapping, back energy transfer and cross-relaxation are different in core and core@shell systems.

Let us take homogenous system UCNP (up-conversion nanoparticles) of NaYF_4 : 2 at.% Er^{3+} -10 at.% Yb^{3+} , which is the best material so far in terms of efficiency at lower laser power excitation at 980 nm (Ningthoujam et al. 2022; Joshi et al. 2021, 2022a, b; Auzel 2004; Ningthoujam unpublished; Johnson et al. 2012; Chaudhuri and Paria 2012; Mahdavi et al. 2020; Huseien 2023). Now, let us take heterogenous system core@shell UCNP nanostructures and possible nanostructures with similar atomic concentrations of Na, Y, Er, Yb and F in each system are $\text{NaYF}_4\text{:Er-Yb@NaYF}_4$, $\text{NaYF}_4\text{@NaYF}_4\text{:Er-Yb}$, $\text{NaYF}_4\text{:Er@NaYF}_4\text{-Yb}$ and $\text{NaYF}_4\text{:Yb@NaYF}_4\text{-Er}$ (Leary et al. 2023). Here, their luminescence intensities are different even when other conditions are fixed in terms of particle size, shape, excitation source and concentration. It means that energy transfer, migration and exchange interaction are different in those heterostructures. Even, if the thickness of shell at the same size

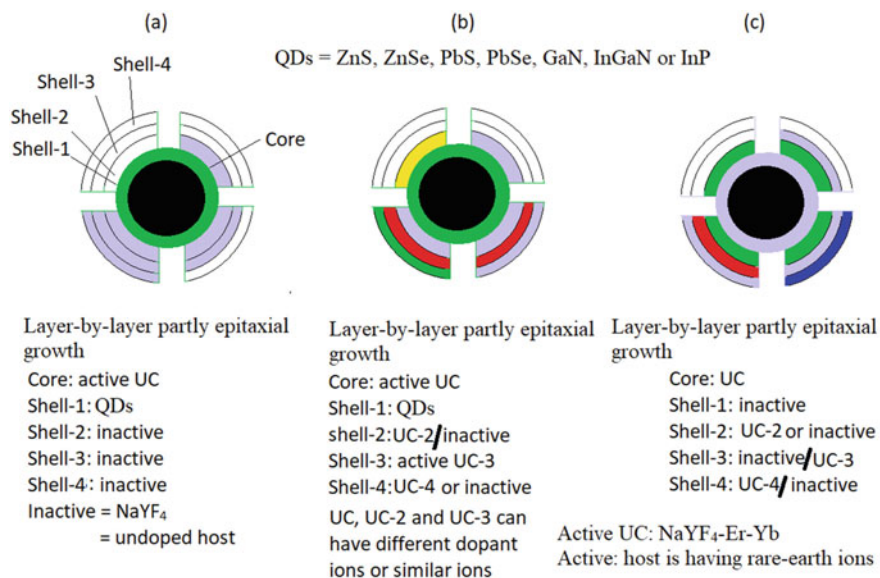


Fig. 2.31 Possible ways for layer-by-layer partly epitaxial growth of core and shell materials. Here, core is active up-converting material. Here, QDs are associated. It is adapted from reference (Ningthoujam unpublished)

of core varies, their properties will change. If another shell (undoped, doped one) is introduced, a more complicated system arises in terms of study.

These core-shell heterostructures have been used in biomedical and pharmaceutical applications, electronics, catalysis, enhancing photoluminescence, tuning of a particular wavelength for a particular application, sensors, creating photonic crystals, data storage, conversion of one isomer to another isomer in light sensitive organic molecules, etc. In the biomedical field, these have been extensively used in imaging, cell labelling, bio-sensing, targeted drug delivery, controlled drug release through light or pH trigger, radio-isotopes based imaging or ac-frequency and therapy and tissue engineering applications, etc. (Ningthoujam et al. 2022; Joshi et al. 2021, 2022a, b; Auzel 2004; Ningthoujam unpublished; Johnson et al. 2012; Chaudhuri and Paria 2012; Mahdavi et al. 2020; Huseien 2023).

2.4 Classes of Core@Shell Nanostructures

Classes of core@shell nanostructures: Core@shell nanostructures can be classified depending on the types of material used in core and shell: This includes the following (Ningthoujam et al. 2022; Joshi et al. 2021, 2022a, b; Auzel 2004; Ningthoujam

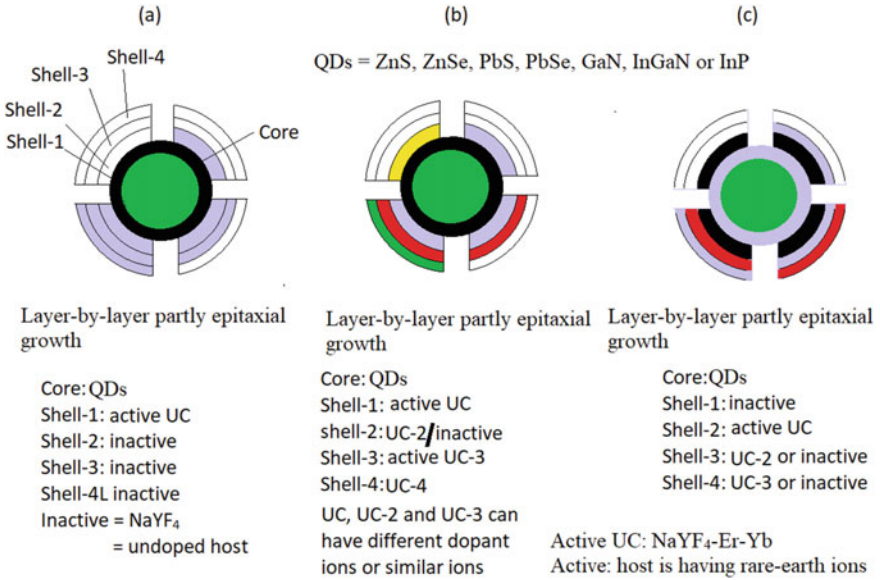


Fig. 2.32 Possible ways for layer-by-layer partly epitaxial growth of core and shell materials. Here, core is inactive such as QDs. It is adapted from reference (Ningthoujam unpublished)

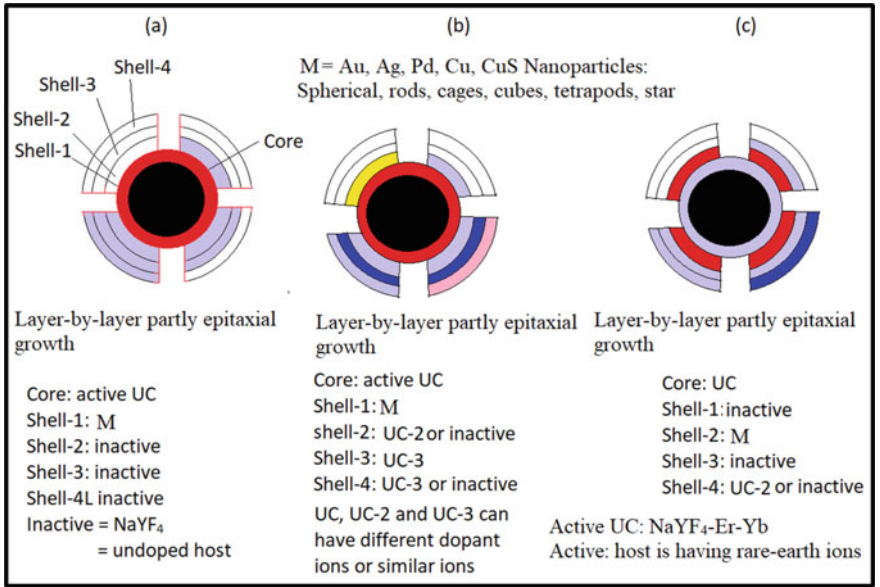


Fig. 2.33 Possible ways for layer-by-layer partly epitaxial growth of core and shell materials. Here, core is active up-converting material. Here, metallic nanoparticles are associated. It is adapted from reference (Ningthoujam unpublished)

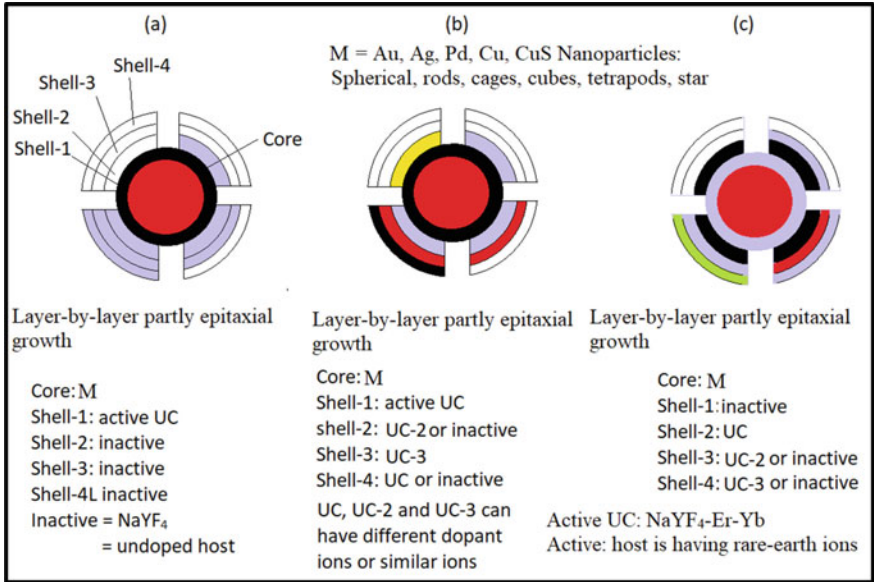


Fig. 2.34 Possible ways for layer-by-layer partly epitaxial growth of core and shell materials. Here, core is inactive such as metallic nanoparticles. It is adapted from reference (Ningthoujam unpublished)

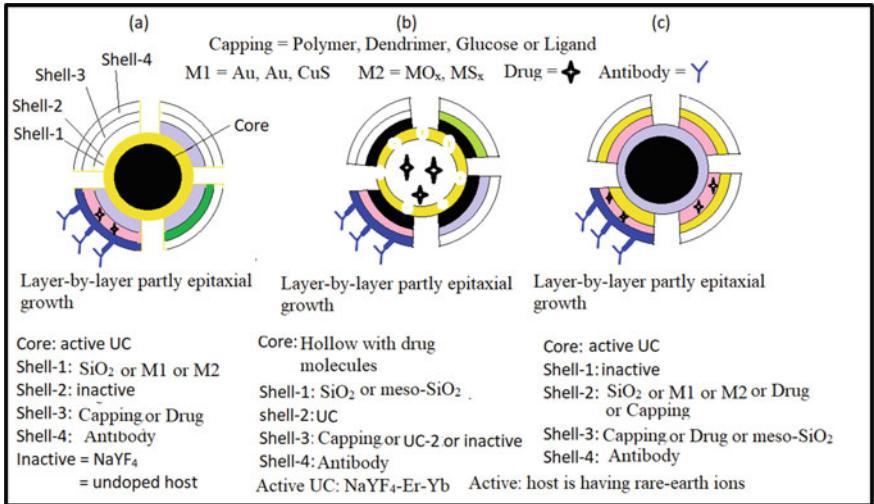


Fig. 2.35 Possible ways for layer-by-layer partly epitaxial growth of core and shell materials. Here, core is active UC or inactive such as metal nanoparticles or metal oxides. Drug and antibody molecules can be loaded. Even radio isotopes can be adsorbed or added. It is adapted from reference (Ningthoujam unpublished)

unpublished; Johnson et al. 2012; Chaudhuri and Paria 2012; Mahdavi et al. 2020; Huseien 2023):

- 2.4.1 Inorganic@inorganic materials
- 2.4.2 Inorganic@organic materials
- 2.4.3 Organic@inorganic materials
- 2.4.4 Organic@organic materials
- 2.4.5 Core@multilayers (shell1@shell2, shell1@shell2@shell3 and so on)
- 2.4.6 Liposome based formulation
- 2.4.7 Dendrimer based formation
- 2.4.8 Hollow core@shell materials

2.4.1 Inorganic@Inorganic materials

Inorganic core can be metal particles such as Au, Ni or different metals (Au, Pt, Pd) or semiconductors (C, CdS, CdSe, Fe₂O₃) or insulators SiO₂. Inorganic shells can be semiconductors or insulators (ZnS, LaF₃, β-NaYF₄:Yb³⁺, Er³⁺, YVO₄-Eu³⁺). It can be happened with opposite trends.

Examples of inorganic@inorganic materials are Au@Ag, Au@SiO₂, Au@C, Au/CdS, Zn@ZnO, Fe₃O₄@Au, Au/Fe₂O₃, Fe₃O₄@SiO₂, PbS@PbSe, ZnS/CdSe, ZnS:Mn/ZnO, Gd₂O₃:Tm³⁺@SiO₂, NaYF₄:Ln@NaYF₄, NaYF₄:Ln@NaGdF₄, NaYF₄:Ln@CaF₂, Fe₃O₄@NaYF₄:Yb-Er, β-NaYF₄:Yb³⁺-Er³⁺@β-NaYF₄, β-NaYF₄:Yb-Tm@β-NaYF₄:Yb-Er, LaF₃@Eu_{0.2}La_{0.8}F₃, LaPO₄:Eu³⁺@LaPO₄, YVO₄-Eu³⁺@YVO₄, YVO₄:Ln@SiO₂, Au@SiO₂@Y₂O₃:Eu³⁺, Fe₃O₄@SiO₂@Al₂O₃, Fe₃O₄@SiO₂@TiO₂, CdSe_xTe_{1-x}@ZnS@SiO₂, CdSe@CdS@ZnS, γ-Fe₂O₃@NaYF₄:Yb-Er, etc.

2.4.2 Inorganic@Organic Materials

Core is inorganic materials such as metals, semiconductors or insulators. Metals are Au, Ag and Fe. Semiconductors are Fe₃O₄, Fe₂O₃, ZrO₂, PbSe, PbS. Insulators are SiO₂, NaYF₄:Ln, CaF₂:Ln. Shell material is organic material. Examples are PEG, PMMA, block polymers, etc.

2.4.3 Organic@Inorganic Materials

Here, organic core is made of organic polymer. A few examples of organic polymer are mentioned here: dextrose, polystyrene, polyurethane, poly(ethylene oxide), poly(vinyl benzyl chloride), poly(vinyl pyrrolidone), surfactants, and different copolymers, such as acrylonitrile-butadiene-styrene, poly-(styreneacrylic acid),

and styrenemethyl methacrylate. Inorganic shells will be metals (Au, Ag), semi-conductors (c-dots, metal oxide TiO_2 , Fe_3O_4 , metal chalcogenide ZnS) or insulators (SiO_2).

2.4.4 *Organic@Organic Materials*

Core particle is made of organic polymer. A few examples of organic polymer are mentioned here: polystyrene (PS), polyphenylene, and poly(D,L-lactic-co-glycolide) (PLGA), poly(N-isopropylacrylamide) (variously abbreviated polymers: PNIPA, PNIPAAm, NIPA, PNIPAA or PNIPAm). Shell particle is organic polymer, such as 1,2-distearoyl-sn-glycero-3-phosphoethanolamine-N-carboxy(poly(ethylene glycol))2000 (DSPE-PEG-COOH), drug, polyethylene oxide (PEO), polyethylene glycol (PEG).

2.4.5 *Core@Multilayers (Shell1@Shell2, Shell1@Shell2@Shell3 and So On)*

Core particle is made of inorganic or organic material. Shell1 with another material (inorganic or organic). Shell2 will be another material. Shell3 will be another material. They shell layer makes multilayers of different materials. Examples are CdSe@CdS@ZnS , CdSe@ZnSe@ZnS , $\text{Au@SiO}_2@Y_2\text{O}_3:\text{Eu}^{3+}$, $\text{LaF}_3:\text{Eu@LnF}_3:\text{Eu}^{3+}@La(\text{NO}_3)_3$, CdSe@CdTe@ZnSe , $\text{CdSe@CdS@Zn}_{0.5}\text{Cd}_{0.5}\text{S@ZnS}$, $\text{InAs}_x\text{P}_{1-x}@InP@ZnSe$, InAs@CdSe@ZnSe , CdSe@HgTe@CdTe , CdS@HgS@CdS , CdSe@CdS@ZnTe , CdS@CdSe@CdS , CdSe@ZnS@CdSe , ZnS@CdS@ZnS , CdS@CdSe@CdS , CdSe@ZnS@CdTe , $\text{Fe}_3\text{O}_4@PGMA@PS$ (here PGMA = poly(glycidyl methacrylate), PS = polystyrene), $\text{Fe}_3\text{O}_4/PEO-PPO-PEO$ block polymer (known as pluronic P123, which consists of a symmetric triblock copolymer comprising poly(ethylene oxide) (PEO) and poly(propylene oxide) (PPO) in an alternating linear fashion, PEO-PPO-PEO and it has a chemical formula $\text{HO}(\text{CH}_2\text{CH}_2\text{O})_{20}(\text{CH}_2\text{CH}(\text{CH}_3)\text{O})_{70}(\text{CH}_2\text{CH}_2\text{O})_{20}\text{H}$), $\gamma\text{-Fe}_2\text{O}_3@PEI + \text{PEO-PGA}$ (PEI = poly-(ethylene amine), PEO-PGA = poly-(ethylene oxide)-poly-(glutamic acid)), iron oxide@ SiO_2 composite@PS, $\text{CoFe}_2\text{O}_4@DTPA-CS$ (DTPA = Diethylenetriamine pentaacetate, CS = chitosan), $\text{Sb}_2\text{O}_3@PMMA@PVC$ (polymethyl methacrylate (PMMA) and polyvinyl chloride (PVC) polymer blend, PEG@Si@Al composite oxide, PS@ $\text{TiO}_2@SiO_2$, PS@styrene and MPS hybrid copolymer, etc.

2.4.6 Liposome Based Formulation

Liposome is a spherical vesicle in which the core is having aqueous medium and shell is having lipid bilayers (hydrophobic). Lipid is generally composed of phospholipids and cholesterol. If one lipid bilayer exists, this is known as uni-lamellar (diameter: 30–100 nm or 100–300 nm). If two or more lipid bilayers exist, this is known as multi-lamellar (diameter = 1–5 μm). Between lipid bilayers, aqueous medium exists. Water soluble/dispersible particles or molecules can be trapped into aqueous core, whereas oil soluble/dispersible particles or molecules can be trapped into lipid bilayers. Au or Fe_3O_4 nanoparticles dispersible in water can be prepared in the core of liposome. Oil soluble Au or Fe_3O_4 nanoparticles can be entrapped in a lipid bilayer (shell). Generally, targeted drug delivery and high accumulation of drugs in cells use the concept of liposome-based system. Luminescent nanomaterial can be trapped into aqueous core and oil-soluble lipid layers depending on the types of nanomaterials.

2.4.7 Dendrimer Based Formation

Dendrimer has highly ordered branched polymeric molecules around the core. Generally, core is hydrophobic whereas outer branched polymeric molecules are hydrophilic. However, core can be modified in order to get functional group such as NH_2 or COOH . In this way, nanoparticles (Au, Fe_3O_4 , ZnS, ZnO in 2–50 nm) can be entrapped into the core (interaction may be ionic or covalent type). Such branched polymeric molecules are soluble in aqueous medium. Nanoparticles encapsulated dendrimers can be used in drug-delivery systems and also agglomeration among nanoparticles is very less.

2.4.8 Hollow Core@Shell Materials

In case, if core@shell nanoparticles are brought to a particular medium or gas medium or laser medium, either core or shell can be removed. Using SIMS experiment or high-power laser, thickness of shell can be decreased. Finally, the shell can be removed. On the other hand, if a particular solvent, which can be capable for soluble only in core material (e.g., Co or Fe core particles can be dissolved into Co^{2+} or $\text{Fe}^{2+}/\text{Fe}^{3+}$ in $\text{pH} < 4$), but not affect the shell, hollow core with shell can be formed. Here core is scarified and shell remains. If metal ions are added to such hollow core@shell in aqueous medium, metal ions enter into the hollow core. When a reducing agent is added, reduction of metal ions to metal nanoparticles can occur. Similarly, if oxidizing agent is added, metal ions can be converted to metal oxide nanoparticles. Such nanoparticles formed can form agglomerated particles inside the core. If the

number of nanoparticles is less, individual particles can exist and can move in the core. Even, luminescent nanoparticles can be generated in the hollow core region.

2.5 Rate of Electronic Decay, Lifetime, Quantum Yield

During electronic transition from ground state to excited state, excited electrons come back to ground state if excitation source is removed. The excitation rate is equal to decay rate. If N_0 is the number of electrons in the ground state and its excited rate is K_A , the number of excited electrons will be N_1 . Decay rate of the excited electrons will be determined by radiative rate (K_R) and non-radiative rate (K_{NR}) (Ningthoujam et al. 2012; Curie 1963; Blasse and Grabmaier 1994; Lakowicz 2006). At a particular time (t), the number of excited electrons can be determined by

$$dN_1/dt = K_A N_0 - (K_R N_1 + K_{NR} N_1) \quad (2.4)$$

When photon of constant intensity is excited, it can achieve a steady state of equilibrium.

Here, $dN_1/dt = 0$.

It implies that

$$N_1 = K_A N_0 / (K_R + K_{NR}) \quad (2.5)$$

And amount of decay at a particular time (t) is given by

$$N_1(t) = N_1 \exp(-K_A t) \quad (2.6)$$

where $K_A = K_R + K_{NR}$.

$$N_1(t)/N_1 = \exp(-K_A t) \quad (2.7)$$

When $K_{NR} = 0$, $N_1 = K_A N_0 / K_R$. In this, lifetime of excited electrons is considered as natural lifetime or intrinsic lifetime (τ_N), which is defined as:

$$\tau_N = 1/K_R \quad (2.8)$$

And $K_A = K_R$.

Intrinsic decay takes place due to collisional interactions among excited electrons.

$$N_1(t)/N_1 = \exp(-K_R t \tau_N) \quad (2.9)$$

$$N_1(t)/N_1 = \exp(-1) = 0.36 \quad (2.10)$$

The nature lifetime (τ_N) is equal to the time required to decay excited electron population to 36%.

The experiment lifetime (τ_{exp}) is generally less than the natural lifetime (τ_N).

$$\tau_{exp} = 1/K_A = 1/(K_R + K_{NR}) \quad (2.11)$$

The fluorescence quantum yield (QY) is the ratio between the fluorescence intensity and light absorb.

$$QY = \text{Photon emitted/Photon absorb} \quad (2.12)$$

$$QY = K_R/(K_R + K_{NR}) \quad (2.13)$$

$$QY = \tau_{exp}/\tau_N \quad (2.14)$$

Here, the source of non-radiative decay is due to the presence of surrounding heat sink or quencher. Due to the transfer of energy from excited electrons, it gives rise to heat to surrounding and thereby multi-phonon relaxation may take place. If $K_{NR} \ll K_R$, luminescence intensity is very high. Luminescence intensity of core activator increases significantly after core-shell formation (shell: inactive or undoped host) due to the increase of distance from core activator to quencher (surface dangling bonds, ligands, solvent, etc.; e.g., core: NaYF₄:Er-Yb and core@shell: NaYF₄:Er-Yb@NaYF₄; and YVO₄:Eu and YVO₄:Eu@YVO₄) (Ningthoujam et al. 2009a, 2022).

2.6 Type of Excitation for Electronic Transitions

There are two ways of excitation: resonance type and non-resonance type (Auzel 2004; Singh 2018). In the resonance type excitation, a large number of electrons go to the excited state having a stable level. In case of non-resonance type, a few electrons go to the excited state having a stable level. Most energy got losses due to the difference between excitation energy and stable energy level and this is provided by multi-phonon relaxation.

However, if high-energy flux (say a few kW/cm²) is provided, situation is different in resonance or non-resonance type process. Sometimes cascades or avalanche phenomenon occurs. Even, continuous or pulse mode excitation changes the process of energy transfer at excited levels.

2.7 Conclusions

Many examples of photo-luminescent materials are provided and their properties such as down-conversion and up-conversion processes are discussed. Many organic compounds, inorganic compounds and organic dyes show the down-conversion process. Many materials showing quantum-cutting process are provided. Different metal complexes, d and f ions doped inorganic compounds show up-conversion process. Possible core@shell nanostructures are mentioned. This helps in the fabrication of devices, light emitting diodes, drug loading, solar cells, energy harvesting, proximity systems, etc. Shape, size and hollowness engineering in nanostructure are mentioned.

References

- Ahmed, S.A.: Structural, optical, and magnetic properties of Mn-doped ZnO samples. *Res. Phys.* **7**, 604–610 (2017)
- Auzel, F.: Upconversion and anti-stokes processes with f and d Ions in Solids. *Chem. Rev.* **104**, 139–173 (2004)
- Blasse, G., Grabmaier, B.C.: *Luminescent Materials*. Springer, Berlin (1994)
- Boens, N., Leen, V., Dehaen, W.: Fluorescent indicators based on BODIPY. *Chem. Soc. Rev.* **41**, 1130–1172 (2012)
- Borse, S., Rafique, R., Murthy, Z.V.P., Park, T.J., Kailasa, S.K.: Applications of upconversion nanoparticles in analytical and biomedical sciences: a review. *Analyst* **147**, 3155–3179 (2022)
- Brabec, C.J., Dyakonov, V., Parisi, J., Sariciftci, N.S.: *Organic Photovoltaics: Concepts and Realization*. Springer-Verlag Berlin Heidelberg (2003)
- Chaganti, L.K., Venkatakrisnan, N., Bose, K.: An efficient method for FITC labelling of proteins using tandem affinity purification. *Biosci. Rep.* **38**, BSR20181764 (2018)
- Chaudhuri, R.G., Paria, S.: Core/shell nanoparticles: classes, properties, synthesis mechanisms, characterization, and applications. *Chem. Rev.* **112**, 2373–2433 (2012)
- Chen, G., Qiu, H., Prasad, P.N., Chen, X.: Upconversion nanoparticles: design, nanochemistry, and applications in theranostics. *Chem. Rev.* **114**, 5161–5214 (2004)
- Chen, R., Hong, Z.F., Zhao, Y.R., Zheng, H., Li, G.J., Zhang, Q.C., Kong, X.J., Long, L.S., Zheng, L.S.: Ligand-dependent luminescence properties of lanthanide-titanium oxo clusters. *Inorg. Chem.* **58**, 15008–15012 (2019)
- Chen, B., Li, D., Wang, F.: InP quantum dots: synthesis and lighting applications. *Small* **16**, 2002454 (2020)
- Chivian, J.S., Case, W.E., Eden, D.D.: The photon avalanche: a new phenomenon in Pr³⁺-based infrared quantum counters. *Appl. Phys. Lett.* **35**, 124 (1979)
- Cravencoco, A., Ye, C., Gräfenstein, J., Börjesson, K.: Interplay between Förster and Dexter energy transfer rates in isomeric donor–bridge–acceptor systems. *J. Phys. Chem. A* **124**, 7219–7227 (2020)
- Curie, D.: *Luminescence in Crystals*, 1st edn. John Wiley & Sons Inc., London (1963)
- da Silva, J.F., da Silva, R.F., Santos, E.P., Maia, L.J.Q., Moura, A.L.: Photon-avalanche-like upconversion in NdAl₃(BO₃)₄ nanoparticles excited at 1064 nm. *Appl. Phys. Lett.* **117**, 151102 (2020)
- Dexter, D.L.: Possibility of luminescent quantum yields greater than unity. *Phys. Rev.* **108**, 630 (1957)

- Dutta, D.P., Ningthoujam, R.S., Tyagi, A.K.: Luminescence properties of Sm³⁺ doped YPO₄: effect of solvent, heat-treatment, Ca²⁺/W⁶⁺-co-doping and its hyperthermia application. *AIP-Adv.* **2**, 042184 (2012)
- Gajbhiye, N.S., Ningthoujam, R.S., Ahmed, A., Panda, D.K., Umre, S.S., Sharma, S.J.: Redispersible Li⁺ and Eu³⁺ co-doped CdS nanoparticles: luminescence studies. *Pramana J. Phys.* **70**, 313 (2008)
- Ganapathi, S.K., Kaur, M., Samanta, S., Datta, N., Singh, A., Ningthoujam, R.S., Gadkari, S.C., Debnath, A.K.: Influence of MgPc modification on NO₂ sensing characteristics of RGTO grown SnO₂ thin films. *Mater. Sci. Semicond. Process.* **152**, 107104 (2022)
- Ghosh, M., Ningthoujam, R.S., Vatsa, R.K., Das, D., Nataraju, V., Gadkari, S.C., Gupta, S.K., Bahadur, D.: Role of ambient air on photoluminescence and electrical conductivity of assembly of ZnO nanoparticles. *J. Appl. Phys.* **110**, 054309 (2011)
- Haider, A.J., Jameel, Z.N., Al-Hussaini, I.H.M.: Review on: titanium dioxide applications. *Energy Procedia* **157**, 17–29 (2019)
- Hasegawa, M., Ohmagari, H., Tanaka, H., Machida, K.: Luminescence of lanthanide complexes: from fundamental to prospective approaches related to water- and molecular-stimuli. *J. Photochem. Photobiol. C* **50**, 100484 (2022)
- Huang, X.Y., Zhang, Q.Y.: Near-infrared quantum cutting via cooperative energy transfer in Gd₂O₃:Bi³⁺, Yb³⁺ phosphors. *J. Appl. Phys.* **107**, 063505 (2010)
- Huseien, G.H.: Potential applications of core-shell nanoparticles in construction industry revisited. *Appl. Nano* **4**, 75–114 (2023)
- Johnson, N.J.J., Korinek, A., Dong, C., van Veggel, F.C.J.M.: Self-focusing by ostwald ripening: a strategy for layer-by-layer epitaxial growth on upconverting nanocrystals. *J. Am. Chem. Soc.* **134**, 11068–11071 (2012)
- Joshi, R., Shelar, S.B., Srivastava, M., Singh, B.P., Goel, L., Ningthoujam, R.S.: Development of core@Shell γ -Fe₂O₃@Mn_xO_y@SiO₂ nanoparticles for hyperthermia, targeting, and imaging applications. *ACS Appl. Bio Mater.* **5**, 5386–5393 (2022a)
- Joshi, R., Patra, S., Srivastava, M., Singh, B.P., Chakraborty, A., Shelar, S.B., Chakravarty, R., Ningthoujam, R.S.: Mesoporous NaGdF₄/Ho–Yb@m-SiO₂ upconversion nanophosphors as a potent theranostic probe. *ACS Appl. Nano Mater.* **5**, 12962–12971 (2022b)
- Joshi, R., Perala, R.S., Shelar, S.B., Ballal, A., Singh, B.P., Ningthoujam, R.S.: Super bright red upconversion in NaErF₄:0.5%Tm@NaYF₄:20%Yb nanoparticles for anti-counterfeit and bio-imaging applications. *ACS Appl. Mater. Interf.* **13**, 3481–3490 (2021)
- Joubert, M.F.: Photon avalanche upconversion in rare earth laser materials. *Opt. Mater.* **11**, 181–203 (1999)
- Karbowiak, M., Mech, A., Drożdżyński, J., Edelstein, N.M.: Crystal-field analysis, upconversion, and excited-state dynamics for (U⁴⁺, U³⁺): Ba₂YCl₇ single crystals. *Phys. Rev. B* **67**, 195108 (2003)
- Kemp, W.: *Organic Spectroscopy*. Macmillan, Pennsylvania State University (1975)
- Kozlov, D.V., Castellano, F.N.: Anti-stokes delayed fluorescence from metal–organic bichromophores. *Chem. Commun.* 2860–2861 (2004)
- Kumari, R., Sunil, D., Ningthoujam, R.S.: Naphthalimides in fluorescent imaging of tumor hypoxia-an up-to-date review. *Bioorg. Chem.* **88**, 102979 (2019a)
- Kumari, R., Vasumathy, R., Sunil, D., Ningthoujam, R.S., Pandey, B.N., Kulkarni, S.D., Varadavenkatesan, T., Venkatachalam, G.A., Anil, N.V.K.: Nitronaphthalimide probe for fluorescence imaging of hypoxia in cancer cells. *J. Fluoresc.* **31**, 1665–1673 (2021)
- Kumari, R., Sunil, D., Ningthoujam, R.S., Pandey, B.N., Kulkarni, S.D., Varadavenkatesan, T., Venkatachalam, G.: Dinitro derivative of naphthalimide as a fluorescent probe for tumor hypoxia imaging. *Polycyclic Aromat. Compd.* **43**, 54–63 (2023)
- Kumari, R., Sunil, D., Ningthoujam, R.S., Kumar, N.V.A.: Azodyes as markers for tumor hypoxia imaging and therapy: an up-to-date review. *Chemico-Biol. Interact.* **307**, 91–104 (2019)

- Lahiri, D., Ningthoujam, R.S., Bhattacharyya, D., Sharma, S.M.: Structural understanding of the spectral characteristics of $\text{SnO}_2:\text{Eu}:\text{Y}_2\text{O}_3$, using extended x-ray absorption fine structure. *J. Appl. Phys.* **107**, 054316 (2010)
- Lakowicz, J.R.: *Principles of Fluorescence Spectroscopy*, 3rd Edn. Springer Science, LLC, Singapore (2006)
- Leary, D.C., Zhang, Y., Rodriguez, J.G., Akhmedov, N.G., Petersen, J.L., Dolinar, B.S., Milsmann, C.: Organometallic intermediates in the synthesis of photoluminescent zirconium and hafnium complexes with pyridine dipyrrolide ligands. *Organometallics* **42**, 1220–1231 (2023)
- Lee, C., Xu, E.Z., Liu, Y., Teitelboim, A., Yao, K., Fernandez-Bravo, A., Kotulska, A.M., Nam, S.H., Suh, Y.D., Bednarkiewicz, A., Cohen, B.E., Chan, E.M., Schuck, P.J.: Giant nonlinear optical responses from photon-avalanching nanoparticles. *Nature* **589**, 230 (2021)
- Levy, E.S., Tajon, C.A., Bischof, T.S., Iafrafi, J., Fernandez-Bravo, A., Garfield, D.J., Chamanzar, M., Maharbiz, M.M., Sohal, V.S., Schuck, P.J., Cohen, B.E.: Energy-looping nanoparticles: harnessing excited-state absorption for deep-tissue imaging. *ACS Nano* **10**(9), 8423 (2016)
- Li, P., Li, H.: Recent progress in the lanthanide-complexes based luminescent hybrid materials. *Coord. Chem. Rev.* **441**, 213988 (2021)
- Li, Y., Wang, T., Ren, W., Han, J., Yin, Z., Qiu, J., Yang, Z., Song, Z.: $\text{BiOCl}:\text{Er}$ nanosheets with tunable thickness for photon avalanche phosphors. *ACS Appl. Nano Mater.* **2**, 7652–7660 (2019)
- Loitongbam, R.S., Singh, N.S., Singh, W.R., Ningthoujam, R.S.: Observation of exceptional strong emission transitions $^5\text{D}_j$ ($j = 1-3$) to $^7\text{F}_j$ ($j = 1-3$): multicolor from single Eu^{3+} ion doped La_2O_3 nanoparticles. *J. Lumin.* **134**, 14–23 (2013)
- Lokesha, H.S., Mohanty, P., Prinsloo, A.R.E., Sheppard, C.J.: Impact of Cr doping on the structure, optical and magnetic properties of nanocrystalline ZnO particles. *J. Alloy. Compd.* **960**, 170815 (2023)
- Longo, V.M., Cavalcante, L.S., Paris, E.C., Sczancoski, J.C., Pizani, P.S., Li, M.S., Andres, J., Longo, E., Varela, J.A.: Hierarchical assembly of CaMoO_4 nano-octahedrons and their photoluminescence properties. *J. Phys. Chem. C* **115**, 5207–5219 (2011)
- Luwang, M.N., Ningthoujam, R.S., Singh, N.S., Tewari, R., Srivastava, S.K., Vatsa, R.K.: Surface chemistry of surfactant AOT-stabilized SnO_2 nanoparticles and effect of temperature. *J. Colloids Interface Sci.* **349**, 27 (2010)
- Mahdavi, Z., Rezvani, H., Moraveji, M.K.: Core-shell nanoparticles used in drug delivery-microfluidics: a review. *RSC Adv.* **10**, 18280–18295 (2020)
- Mamiyev, Z., Balayeva, N.O.: PbS nanostructures: a review of recent advances. *Mater. Today Sustain.* **21**, 100305 (2023)
- Meetei, S.D., Singh, S.D., Singh, N.S., Sudarsan, V., Ningthoujam, R.S., Tyagi, M., Gadkari, S.C., Tewari, R., Vatsa, R.K.: Crystal structure and photoluminescence correlations in white emitting nanocrystalline $\text{ZrO}_2:\text{Eu}^{3+}$ phosphor: effect of doping and annealing. *J. Lumin.* **132**, 537–544 (2012)
- Mir, W.J., Sheikh, T., Arfin, H., Xia, Z., Nag, A.: Lanthanide doping in metal halide perovskite nanocrystals: spectral shifting, quantum cutting and optoelectronic applications. *NPG Asia Mater.* **12**, 9 (2020)
- Ningthoujam, R.S.: Generation of exciton in two semiconductors interface: $\text{SnO}_2:\text{Eu}-\text{Y}_2\text{O}_3$. *Chem. Phys. Lett.* **497**, 208 (2010)
- Ningthoujam, R.S.: Enhancement of luminescence by rare earth ions doping in semiconductor host. In: Rai, S.B., Dwivedi, Y. (eds.) *Synthesis, Characterization and Applications of Multifunctional Materials Material Science and Technologies*, Chapter 7, pp. 145–182. Nova Science Publishers Inc., USA (2012)
- Ningthoujam, R.S., Kulshreshtha, S.K.: Nanocrystalline SnO_2 from thermal decomposition of tin citrate crystal: luminescence and Raman studies. *Mater. Res. Bull.* **44**, 57 (2009)
- Ningthoujam, R.S., Lahiri, D., Sudarsan, V., Poswal, H.K., Kulshreshtha, S.K., Sharma, S.M., Bhushan, B., Sastry, M.D.: Nature of V^{n+} ions in SnO_2 : EPR and photoluminescence studies. *Mater. Res. Bull.* **42**, 1293 (2007a)

- Ningthoujam, R.S., Sudarsan, V., Godbole, S.V., Kienle, L., Kulshreshtha, S.K., Tyagi, A.K.: SnO₂:Eu³⁺ nanoparticles dispersed in TiO₂ matrix: Improved energy transfer between semiconductor host and Eu³⁺ ions for the low temperature synthesized samples. *Appl. Phys. Lett.* **90**, 173113 (2007b)
- Ningthoujam, R.S., Sudarsan, V., Kulshreshtha, S.K.: SnO₂: Eu nanoparticles dispersed in silica: a low temperature synthesis and photoluminescence study. *J. Lumin.* **127**, 747 (2007c)
- Ningthoujam, R.S., Sudarsan, V., Vinu, A., Srinivasu, P., Ariga, K., Kulshreshtha, S.K., Tyagi, A.K.: Luminescence properties of SnO₂ nanoparticles dispersed in Eu³⁺ doped SiO₂. *J. Nanosci. Nanotech.* **8**, 1489 (2008a)
- Ningthoujam, R.S., Gajbhiye, N.S., Ahmed, A., Umre, S.S., Sharma, S.J.: Re-dispersible Li⁺ and Eu³⁺ co-doped nanocrystalline ZnO: luminescence and EPR studies. *J. Nanosci. Nanotech.* **8**, 3059 (2008b)
- Ningthoujam, R.S., Singh, L.R., Sudarsan, V., Singh, S.D.: Energy transfer process and optimum emission studies in luminescence of core-shell nanoparticles: YVO₄:Eu-YVO₄ and surface state analysis. *J. Alloys Comp.* **484**, 782 (2009a)
- Ningthoujam, R.S., Vatsa, R.K., Vinu, A., Ariga, K., Tyagi, A.K.: Room temperature exciton formation in SnO₂ nanocrystals in SiO₂: Eu matrix: quantum dot system, heat-treatment effect. *J. Nanosci. Nanotech.* **9**, 2634 (2009b)
- Ningthoujam, R.S., Sudarsan, V., Vatsa, R.K., Kadam, R.M., Jagannath, G.A.: Photoluminescence studies on Eu doped TiO₂ nanoparticles. *J. Alloys Comp.* **486**, 864 (2009c)
- Ningthoujam, R.S., Gautam, A., Padma, N.: Oleylamine as reducing agent in syntheses of magic-size clusters and monodisperse quantum dots: optical and photoconductivity studies. *Phys. Chem. Chem. Phys.* **19**, 2294–2303 (2017)
- Ningthoujam, R.S.: Finding confined water in hexagonal phase of Bi_{0.05}Eu_{0.05}Y_{0.90}PO₄.xH₂O and its impact for identifying the location of luminescence quencher. *Pramana J. Phys.* **80**, 1055 (2013)
- Ningthoujam, R.S., Joshi, R., Srivastava, M.: Frequency upconversion in core@shell nanoparticles. In: Rai, V.K. (ed) *Upconverting Nanoparticles: From Fundamentals to Applications*. Wiley (2022)
- Ningthoujam RS, Core-shell nanostructures, proximity effect and its applications (unpublished)
- Okram, R., Yaiphaba, N., Ningthoujam, R.S., Singh, N.R.: Is higher ratio of monoclinic to tetragonal in LaVO₄ a better luminescence host? Redispersion and polymer film formation. *Inorg. Chem.* **53**, 7204–7213 (2014)
- Omelon, S., Georgiou, J., Habraken, W.: A cautionary (spectral) tail: red-shifted fluorescence by DAPI–DAPI interactions. *Biochem. Soc. Trans.* **44**, 46–49 (2016)
- Pan, G.H., Wu, H., He, S., Zhang, L., Hao, Z., Zhanga, X., Zhang, J.: Dye-embedded YAG:Ce³⁺@SiO₂ composite phosphors toward warm wLEDs through radiative energy transfer: preparation, characterization and luminescence properties. *Nanoscale* **10**, 22237–22251 (2018)
- Parchur, A.K., Ningthoujam, R.S.: Preparation, microstructure and crystal structure studies of Li⁺ co-doped YPO₄:Eu³⁺. *RSC Adv.* **2**, 10854–10858 (2012a)
- Parchur, A.K., Ningthoujam, R.S.: Behaviour of electric and magnetic dipole transitions of Eu³⁺, ⁵D₀→⁷F₀ and Eu-O charge transfer band in Li⁺ co-doped YPO₄:Eu³⁺. *RSC Adv.* **2**, 10859–10868 (2012b)
- Parchur, A.K., Prasad, A.I., Rai, S.B., Ningthoujam, R.S.: Improvement of blue, white and NIR emissions in YPO₄:Dy³⁺ nanoparticles on co-doping of Li⁺ ions. *Dalton Trans. Commun.* **41**, 13810 (2012a)
- Parchur, A.K., Prasad, A.I., Rai, S.B., Tewari, R., Sahu, R.K., Okram, G.S., Singh, R.A., Ningthoujam, R.S.: Observation of intermediate bands in Eu³⁺ doped YPO₄ host: Li⁺ ion effect and blue to pink light emitter. *AIP Adv.* **2**, 032119 (2012b)
- Parchur, A.K., Ansari, A.A., Singh, B.P., Hasan, T.N., Syed, N.A., Rai, S.B., Ningthoujam, R.S.: Enhanced luminescence of CaMoO₄: Eu by core@shell formation and its hyperthermia study after hybrid formation with F₆C₃O₄: cytotoxicity assessing on human liver cancer cells and mesenchymal stem cells. *Integr. Biol.* **6**, 53–64 (2014)

- Peng, Y., Xu, L., Peng, J., Wang, T., Wang, Q., Li, Y., Yin, Z., Han, J., Qiu, J., Yang, Z., Song, Z.: Enhanced upconversion luminescence in layered $\text{Bi}_2\text{GdO}_4\text{Cl}:\text{Yb}^{3+}/\text{Er}^{3+}$ by reducing OV's and its application in photocatalysis. *J. Lumin.* **252**, 119269 (2022)
- Phaomei, G., Ningthoujam, R.S., Singh, W.R., Singh, N.S., Luwang, M.N., Tewari, R., Vatsa, R.K.: Low temperature synthesis and luminescence properties of re-dispersible Eu^{3+} doped LaPO_4 nanorods by ethylene glycol route. *Opt. Mater.* **32**, 616 (2010)
- Phaomei, G., Ningthoujam, R.S., Singh, W.R., Loitongbam, R.S., Singh, N.S., Rath, A., Juluri, R.R., Vatsa, R.K.: Luminescence switching behaviour through redox reaction in Ce^{3+} co-doped $\text{LaPO}_4:\text{Tb}^{3+}$ nanorods: re-dispersible and polymer film. *Dalton Trans.* **40**, 11571 (2011a)
- Phaomei, G., Singh, W.R., Ningthoujam, R.S.: Solvent effect in monoclinic to hexagonal phase transformation in $\text{LaPO}_4:\text{RE}$ ($\text{RE} = \text{Dy}^{3+}, \text{Sm}^{3+}$) nanoparticles: photoluminescence study. *J. Lumin.* **131**, 1164 (2011b)
- Phaomei, G., Singh, W.R., Singh, N.S., Ningthoujam, R.S.: Luminescence properties of Ce^{3+} co-activated $\text{LaPO}_4:\text{Dy}^{3+}$ nanorods prepared in different solvents and tunable blue to white light emission from Eu^{3+} co-activated $\text{LaPO}_4:\text{Dy}^{3+}, \text{Ce}^{3+}$. *J. Lumin.* **134**, 649–656 (2013)
- Piper, W.W., DeLuca, J.A., Ham, F.S.: Cascade fluorescent decay in Pr^{3+} -doped fluorides: achievement of a quantum yield greater than unity for emission of visible light. *J. Lumin.* **8**, 344–348 (1974)
- Prasad, A.I., Parchur, A.K., Juluri, R.R., Jadhav, N., Pandey, B.N., Ningthoujam, R.S., Vatsa, R.K.: Bi-functional properties of $\text{Fe}_3\text{O}_4@ \text{YPO}_4$: Eu hybrid nanoparticles: hyperthermia application. *Dalton Trans.* **42**, 4885–4896 (2013)
- Rao, C.M., Sudarsan, V., Ningthoujam, R.S., Gautam, U.K., Vatsa, R.K., Vinu, A., Tyagi, A.K.: Luminescence studies on low temperature synthesized $\text{ZnGa}_2\text{O}_4:\text{Ln}^{3+}$ ($\text{Ln} = \text{Tb}$ and Eu) nanoparticles. *J. Nanosci. Nanotech.* **8**, 5776 (2008)
- Sahu, R.K., Ganguly, K., Mishra, T., Mishra, M., Ningthoujam, R.S., Roy, S.K., Pathak, L.C.: Stabilization of intrinsic defects at high temperatures in ZnO nanoparticles by Ag. *J. Colloid Interf. Sci.* **366**, 8–15 (2012a)
- Sahu, N.K., Ningthoujam, R.S., Bahadur, D.: Disappearance and recovery of luminescence in $\text{GdPO}_4:\text{Eu}^{3+}$ nanorods: propose to water/ OH^- release under near infrared and gamma irradiations. *J. Appl. Phys.* **112**, 014306 (2012)
- Sahu, N.K., Shanta Singh, N., Ningthoujam, R.S., Bahadur, D.: Ce^{3+} sensitized $\text{GdPO}_4:\text{Tb}^{3+}$ nanorods: an investigation on energy transfer, luminescence switching and quantum yield. *ACS Photonics* **1**, 337–346 (2014)
- Shalav, A., Richards, B.S., Green, M.A.: Luminescent layers for enhanced silicon solar cell performance: up-conversion. *Sol. Energy Mater. Sol. Cells* **91**, 829–842 (2007)
- Shao, Q., Zhang, G., Ouyang, L., Hu, Y., Donga, Y., Jiang, J.: Emission color tuning of core/shell upconversion nanoparticles through modulation of laser power or temperature. *Nanoscale* **9**, 12132–12141 (2017)
- Sharma, K.S., Melwani, P.K., Yadav, H.D., Joshi, R., Shetake, N.G., Dubey, A.K., Singh, B.P., Phapale, S., Phadnis, P.P., Vatsa, R.K., Ningthoujam, R.S., Pandey, B.N.: Deoxyglucose-conjugated persistent luminescent nanoparticles for theragnostic application in fibrosarcoma tumor model. *RSC Adv.* **13**, 13240–13251 (2023)
- Sheen, M., Ko, Y., Kim, D.U., Kim, J., Byun, J.H., Choi, Y.S., Ha, J., Yeon, K.Y., Kim, D., Jung, J., Choi, J., Kim, R., Yoo, J., Kim, I., Joo, C., Hong, N., Lee, J., Jeon, S.H., Oh, S.O., Lee, J., Ahn, N., Lee, C.: Highly efficient blue InGaN nanoscale light-emitting diodes. *Nature* **608**, 56–61 (2022)
- Shetty, D., Kim, Y.J., Shim, H., Snyder, J.P.: Eliminating the heart from the curcumin molecule: monocarbonyl curcumin mimics (MACs). *Molecules* **20**, 249–292 (2015)
- Shukla, R., Ningthoujam, R.S., Tyagi, A.K., Vatsa, R.K.: Luminescence properties of Dy^{3+} doped Gd_2O_3 nanoparticles prepared by glycine route: annealing effect. *Int. J. Nanotechnol.* **7**, 843 (2010)
- Simmons, J.H., Potter, K.S.: *Optical Materials*. Academic Press, New York (2000)

- Singh, P.: Optical properties of rare earth doped phosphors and hybrid materials (Doctoral thesis). Banaras Hindu University, UP, India (2018)
- Singh, L.R., Ningthoujam, R.S.: Critical view on energy transfer, site symmetry, improvement in luminescence of Eu^{3+} , Dy^{3+} doped YVO_4 by core-shell formation. *J. Appl. Phys.* **107**, 104304 (2010)
- Singh, L.R., Ningthoujam, R.S.: Critical view on luminescence properties of $\text{Y}_2\text{O}_3:\text{Eu}^{3+}$ after dispersion in SiO_2 . *Chem. Phys. Lett.* **510**, 120 (2011)
- Singh, L.R., Ningthoujam, R.S., Sudarsan, V., Singh, S.D., Kulshreshtha, S.K.: Probing of surface Eu^{3+} ions present in $\text{ZnO}:\text{Eu}$ nanoparticles by covering $\text{ZnO}:\text{Eu}$ core with Y_2O_3 shell: luminescence study. *J. Lumin.* **128**, 1544 (2008a)
- Singh, N.S., Ningthoujam, R.S., Devi, L.R., Yaiphaba, N., Sudarsan, V., Singh, S.D., Vatsa, R.K., Tewari, R.: Luminescence study of Eu^{3+} doped GdVO_4 nanoparticles: concentration, particle size and core-shell effects. *J. Appl. Phys.* **104**, 104307 (2008b)
- Singh, L.R., Ningthoujam, R.S., Singh, S.D.: Tuning of ultra-violet to green emission by choosing suitable excitation wavelength in $\text{ZnO}:\text{Eu}$ quantum dot, nanocrystals and bulk. *J. Alloys Comp.* **487**, 466 (2009a)
- Singh, N.S., Ningthoujam, R.S., Yaiphaba, N., Singh, S.D., Vatsa, R.K.: Lifetimes and quantum yield studies of Dy^{3+} doped GdVO_4 : concentrations and annealing effect. *J. Appl. Phys.* **105**, 064303 (2009b)
- Singh, L.R., Ningthoujam, R.S., Singh, N.S., Singh, S.D.: Probing Dy^{3+} ions on the surface of nanocrystalline YVO_4 : luminescence study. *Opt. Mater.* **32**, 286 (2009c)
- Singh, N.S., Ningthoujam, R.S., Singh, S.D., Viswanadh, B., Manoj, N., Vatsa, R.K.: Preparation of highly crystalline blue emitting $\text{MVO}_4:\text{Tm}^{3+}$ ($\text{M} = \text{Gd}, \text{Y}$) spherical nanoparticles: effects of activator concentration and annealing temperature on luminescence, lifetime and quantum yield. *J. Lumin.* **130**, 2452 (2010)
- Singh, N.S., Ningthoujam, R.S., Phaomei, G., Singh, G.D., Vinu, A., Vatsa, R.K.: Re-dispersion and film formation of $\text{GdVO}_4:\text{Ln}^{3+}$ ($\text{Ln}^{3+} = \text{Dy}^{3+}, \text{Eu}^{3+}, \text{Sm}^{3+}, \text{Tm}^{3+}$) nanoparticles: particle size and luminescence studies. *Dalton Trans.* **41**, 4404 (2012)
- Singh, B.P., Parchur, A.K., Ningthoujam, R.S., Ansari, A.A., Singh, P., Rai, S.B.: Influence of Gd^{3+} co-doping on structural property of $\text{CaMoO}_4:\text{Eu}$. *Dalton Trans.* **43**, 4770–4778 (2014a)
- Singh, L.P., Srivastava, S.K., Mishra, R., Ningthoujam, R.S.: Multifunctional hybrid nanomaterials from water dispersible $\text{CaF}_2:\text{Eu}^{3+}$, Mn^{2+} and Fe_3O_4 for luminescence and hyperthermia application. *J. Phys. Chem. C* **118**, 18087–18096 (2014b)
- Singh, L.P., Jadhav, N.V., Sharma, S., Pandey, B.N., Srivastava, S.K., Ningthoujam, R.S.: Hybrid nanomaterials $\text{YVO}_4:\text{Eu}/\text{Fe}_3\text{O}_4$ for optical imaging and hyperthermia in cancer cells. *J. Mater. Chem. C* **3**, 1965–1975 (2015)
- Singh-Rachford, T.N., Castellano, F.N.: Photon upconversion based on sensitized triplet–triplet annihilation. *Coord. Chem. Rev.* **254**, 2560–2573 (2010)
- Sommerdijk, J.L., Bril, A., de Jager, A.W.: Two photon luminescence with ultraviolet excitation of trivalent praseodymium. *J. Lumin.* **8**, 341–343 (1974)
- Srinivasu, K., Ningthoujam, R.S., Sudarsan, V., Vatsa, R.K., Tyagi, A.K., Srinivasu, P., Vinu, A.: Eu^{3+} and Dy^{3+} doped YPO_4 nanoparticles: low temperature synthesis and luminescence studies. *J. Nanosci. Nanotech.* **9**, 3034 (2009)
- Srivastava, M., Devi, L.S., Joshi, R., Singh, B.P., Ningthoujam, R.S.: Effect of signal to noise ratio on luminescence property of $\text{YPO}_4:\text{Eu}$. *Mater. Lett. X* **16**, 100170 (2022)
- Srite, S., Morkoç, T.: GaN , AlN , and InN : a review. *J. Vac. Sci. Technol.*, B **10**, 1237–1266 (1992)
- Tai, C.L., Hong, W.L., Kuo, Y.T., Chang, C.Y., Niu, M.C., Ochathevar, M.K.P., Hsu, C.L., Horng, S.F., Chao, Y.C.: Ultrastable, deformable, and stretchable luminescent organic-inorganic perovskite nanocrystal-polymer composites for 3D printing and white light-emitting diodes. *ACS Appl. Mater. Interfaces* **11**, 30176–30184 (2019)
- Takizawa, Y., Kamada, K., Yoshino, M., Yamaji, A., Kurosawa, S., Yokota, Y., Sato, H., Toyoda, S., Ohashi, Y., Hanada, T., Kochurikhin, V.V., Yoshikawa, A.: Growth and scintillation properties of Tl -doped $\text{CsI}/\text{CsCl}/\text{NaCl}$ ternary eutectic scintillators. *Jpn. J. Appl. Phys.* **60**, SBBK01 (2021)

- Tanner, P.A., Pan, Z.: Luminescence properties of lanthanide and transition metal ion-doped $\text{Ba}_2\text{LaNbO}_6$: detection of MnO_6^{8-} and CrO_6^{9-} clusters. *Inorg. Chem.* **48**, 11142–11146 (2009)
- Wang, Y., Shi, J., Chen, J., Zhu, W., Baranoff, E.: Recent progress in luminescent liquid crystal materials: design, properties and application for linearly polarised emission. *J. Mater. Chem. C* **3**, 7993–8005 (2015)
- Wang, J., Zhang, J., Zhou, Y., Liu, H., Xue, Q., Li, X., Chueh, C.C., Yip, H.L., Zhu, Z., Jen, A.K.Y.: Highly efficient all-inorganic perovskite solar cells with suppressed non-radiative recombination by a Lewis base. *Nat. Commun.* **11**, 177 (2020)
- Wegeberg, C., Wenger, O.S.: Luminescent first-row transition metal complexes. *JACS Au* **1**, 1860–1876 (2021)
- Wegh, R.T., Donker, H., Meijerink, A., Lamminmaki, R.J., Holsa, J.: Vacuum-ultraviolet spectroscopy and quantum cutting for Gd^{3+} in LiYF_4 . *Phys. Rev. B* **56**, 13841 (1997)
- Wegh, R.T., Donker, H., Oskam, K.D., Meijerink, A.: Visible quantum cutting in $\text{LiGdF}_4:\text{Eu}^{3+}$ through downconversion. *Science* **283**, 664 (1999)
- Xie, L., Wang, Y., Zhang, H.: Near-infrared quantum cutting in $\text{YPO}_4:\text{Yb}^{3+}, \text{Tm}^{3+}$ via cooperative energy transfer. *Appl. Phys. Lett.* **94**, 061905 (2009)
- Xie, C., Xie, S., Yi, R., Cao, R., Yuan, H., Xiao, F.: Site-selective occupation for broadband upconversion luminescence in $\text{Ca}_3\text{Y}(\text{GaO})_3(\text{BO}_3)_4:\text{Yb}^{3+}, \text{Mn}^{2+}$ phosphors. *J. Phys. Chem. C* **124**, 6845–6852 (2020)
- Yadav, R.S., Ningthoujam, R.S.: Synthesis and characterization of quantum cutting phosphor materials. In: Tyagi, A.K., Ningthoujam, R.S. (eds.) *Handbook on Synthesis Strategies for Advanced Material: Volume-III: Materials specific synthesis strategies*, Chapter 7, pp. 213–250. Springer Nature, Singapore (2021)
- Yaiphaba, N., Ningthoujam, R.S., Singh, N.S., Vatsa, R.K., Singh, N.R.: Probing of inversion symmetry site in Eu^{3+} doped GdPO_4 by luminescence study: concentration and annealing effect. *J. Lumin.* **130**, 174 (2010a)
- Yaiphaba, N., Ningthoujam, R.S., Singh, N.S., Vatsa, R.K., Singh, N.R., Dhara, S., Misra, N.L., Tewari, R.: Luminescence, lifetime, and quantum yield studies of redispersible Eu^{3+} -doped GdPO_4 crystalline nanoneedles: core-shell and concentration effects. *J. Appl. Phys.* **107**, 034301 (2010c)
- Yaiphaba, N., Ningthoujam, R.S., Singh, N.R., Vatsa, R.K.: Luminescence properties of redispersible Tb^{3+} -Doped GdPO_4 nanoparticles prepared by an ethylene glycol route. *Eur. J. Inorg. Chem.* 2682 (2010)
- Ye, S., Song, E.H., Zhang, Q.Y.: Transition metal-involved photon upconversion. *Adv. Sci.* **3**, 1600302 (2016)
- Ye, H.Y., Tang, Y.Y., Li, P.F., Liao, W.Q., Gao, J.X., Hua, X.N., Cai, H., Shi, P.P., You, Y.M., Xiong, R.G.: Metal-free three-dimensional perovskite ferroelectrics. *Science* **361**, 151–155 (2018)
- Zhang, Q.Y., Huang, X.Y.: Recent progress in quantum cutting phosphors. *Prog. Mater. Sci.* **55**, 353–427 (2010)
- Zhuang, Y., Katayama, Y., Ueda, J., Tanabe, S.: A brief review on red to near-infrared persistent luminescence in transition-metal-activated phosphors. *Opt. Mater.* **36**, 1907–1912 (2014)
- Zou, Z., Feng, L., Cao, C., Zhang, J., Wang, Y.: Near-infrared quantum cutting long persistent luminescence. *Sci. Rep.* **6**, 24884 (2016)